

Imaging of spinal cord compression

A wide spectrum of conditions may compress the spinal cord: degenerative disease, disc herniation and neoplasms are the most common causes; other conditions include trauma, epidural abscess and hematoma. The role of imaging is to establish a radiological diagnosis, to distinguish intrinsic spinal cord disease from extrinsic compression, to define mechanical spine stability and to evaluate the integrity of neural tissue. Clinical presentation, variable in severity and patterns of progression, influences the imaging approach. Imaging is required to assess osseous structures and soft tissues. The need to image 'across anatomical compartments' usually requires more than one imaging technique. Multidetector CT is the first-line imaging modality in acute spine trauma. MRI is the best imaging modality to assess soft tissues, image the extradural, intradural and spinal cord compartments. MRI needs to be implemented with fat-suppression techniques applied to T_2 - and contrast-enhanced T_1 -weighted sequences. MRI helps predict neurological recovery, providing macroscopic information including both reversible and irreversible histologic changes. Diffusion tensor imaging enables depiction of microstructural changes in the compressed spinal cord, which could further predict tissue viability, and functional prognosis. The role of CT myelography is reserved to selected cases, when MRI is not feasible or results are unclear but, intrathecal injection of contrast from below and above the compression level might be necessary to overcome the diagnostic limitations imposed by a myelographic block. This article summarizes the capabilities and limits of different imaging modalities in the spinal cord compression scenario, suggesting technical imaging protocols and diagnostic pathways, and discusses imaging aspects of various causes of spinal cord compression, following an organization based on their anatomical compartment of origin: osseous, epidural or intradural.

Keywords: compression • CT • differential diagnosis • imaging • magnetic resonance • myelopathy • myelo-CT • neoplasms • spinal cord injury

Background

Spinal cord compression (SCC) is a medical emergency that requires immediate imaging assessment and appropriate treatment to prevent or minimize neurologic sequelae that could potentially be devastating.

Clinical presentation

SCC can manifest with a wide range of clinical presentations, course and degrees of severity. Standardized classification of neurological impairment is stated by the

American Spinal Injury Association; such worldwide standards facilitate clinical patient care, as well as research in spinal cord injury medicine [1].

Generally, patients with SCC have a combination of motor and sensory dysfunction with a segmental distribution referable to one or few contiguous spinal levels [2]. Quadriplegia represents the most serious presentation and, depending on the level of the spinal lesion, there may also be respiratory failure. Acute or severe SCC may also

Daniela Distefano*¹
& Alessandro Cianfoni¹

¹Neuroradiology, Neurocenter of Southern Switzerland, NSI, Ospedale Regionale di Lugano, Via Tesserete 46, 6900, Lugano, Switzerland

*Author for correspondence:
Tel.: +41 091 811 60 46
Fax: +41 091 811 69 15
daniela_distefano@hotmail.it

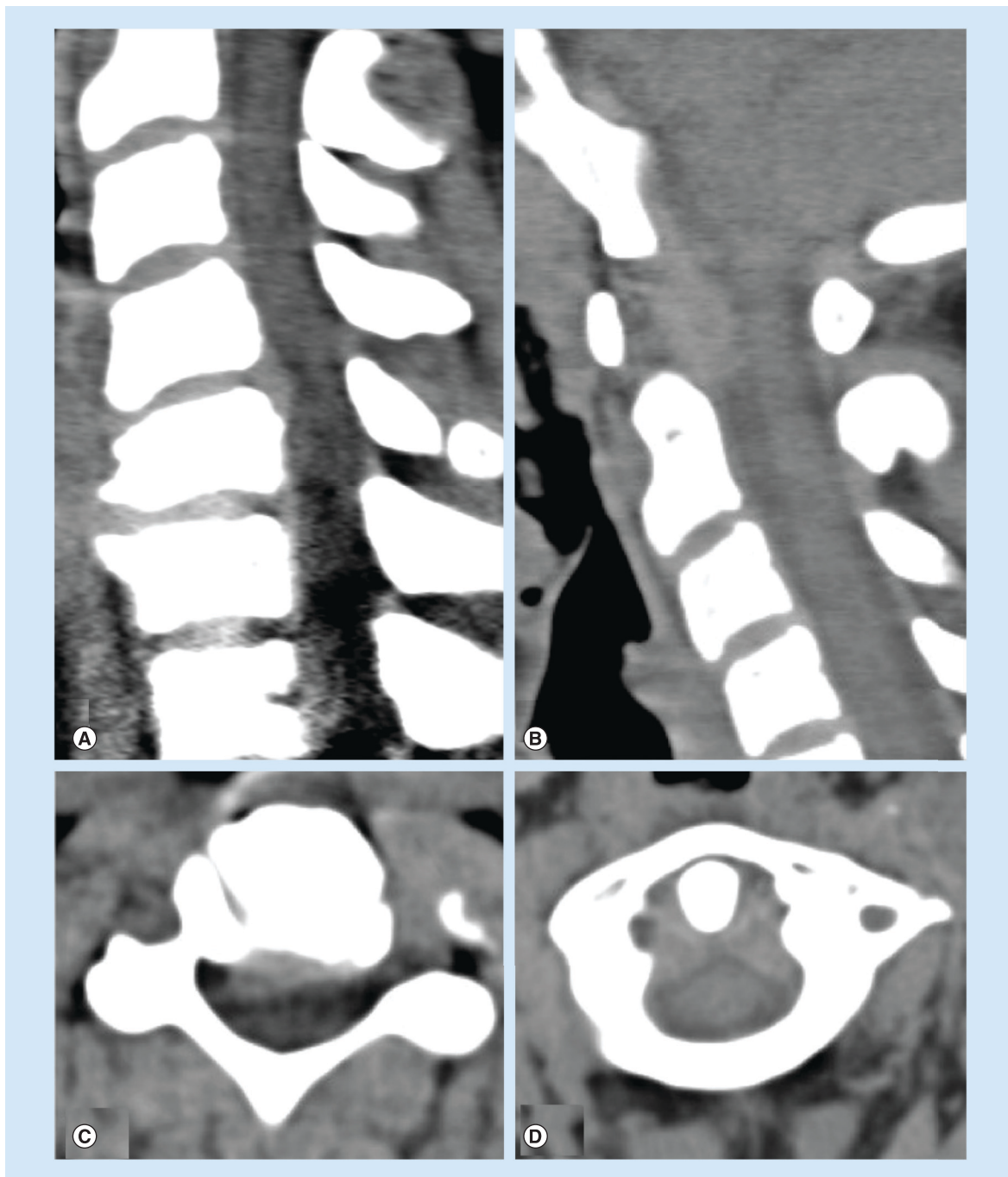


Figure 1. Soft tissues abnormality visualization on CT images. (A & B) Sagittal reformatted and axial CT images show a right posterior paramedian C4–C5 disk herniation with encroachment on the central canal; (C & D) sagittal reformatted and axial CT images demonstrate hyperdense thickening of periodontoideum soft tissue consistent with a post-traumatic epidural hematoma.

cause paraparesis or quadriparesis, hyporeflexia followed by hyperreflexia, extensor plantar responses, loss of sphincter tone and sensory deficits. The sensory deficit, with its most cranial involved dermatome, often marks the SCC level (sensory level). Progressive, generally nontraumatic SCC, may initially be associated with different and less specific symptoms,

such as back pain, usually followed by the onset of radicular pain symptoms, weakness, sensory loss and changes in sphincter function. Gait disturbance and stumbling can be early symptoms of impending neurologic loss [3]. Urinary retention, secondary to autonomic dysfunction, is the most common bladder complaint, along with saddle distribution sensory loss,

for patients with evolving conus medullaris or cauda equina syndrome.

Why imaging?

To confirm a clinically suspected SCC, it is mandatory to perform an imaging work-up. The role of imaging is fundamental to establish a radiological diagnosis, to distinguish intrinsic spinal cord disease from extrinsic cord compression, to define mechanical spine stability, to evaluate the integrity of neural tissue, to provide further radiological information, and to guide treatment if necessary [4].

Imaging techniques

Imaging approaches rely on clinical features and anamnestic criteria. The appropriate use of each avail-

able imaging modality is based on the clinical setting, the complexity of spine anatomy and the relative capabilities/limits of each technique.

The spine is a complex anatomical environment and, in the setting of SCC, imaging is requested to assess osseous structures and soft tissues, as muscles, discs, ligaments, epidural fat planes, meninges, cerebrospinal fluid (CSF), vessels and spinal cord. The need to image 'across anatomical compartments' usually requires more than one imaging technique to establish a final diagnosis [4].

Plain film radiography

Plain films represent the most accessible and less expensive imaging modality in spinal disorders. In general, plain films are acquired in a minimum of two

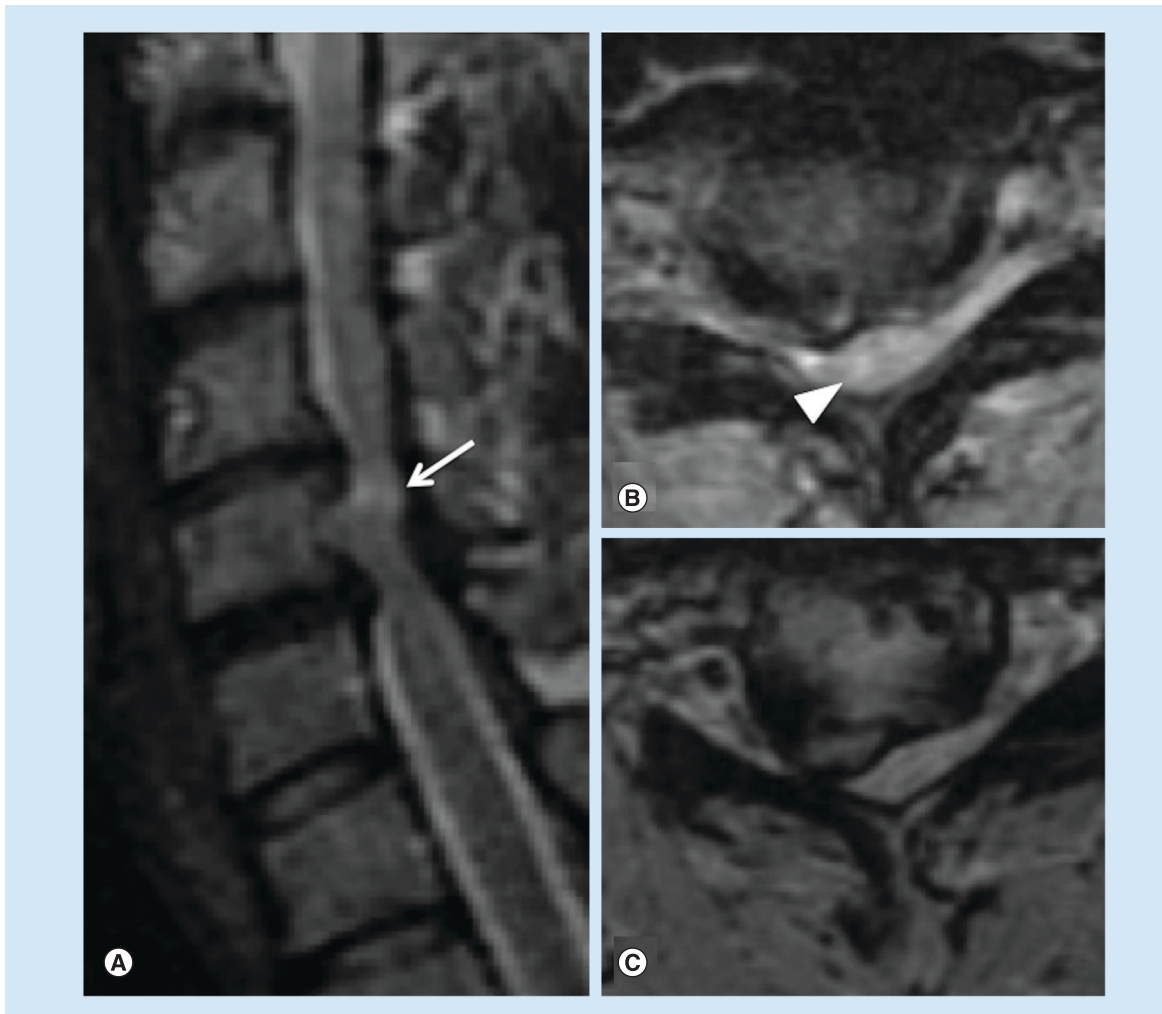


Figure 2. Spondylotic compressive changes with myelomalacia. (A) Sagittal T_2 -weighted turbo spin echo image shows degenerative cervical spondylotic changes causing spinal cord compression at two adjacent levels, with intramedullary focal well-defined hyperintense signal in the cord (arrow in A), indicative of chronic compressive myelopathy with gliosis and myelomalacia; (B & C) axial gradient-recalled echo T_2^* -weighted images confirm the abnormal intramedullary signal (arrowhead in B) and show the degree of central canal stenosis and cord compression at the two levels, due to right paracentral disk herniations.

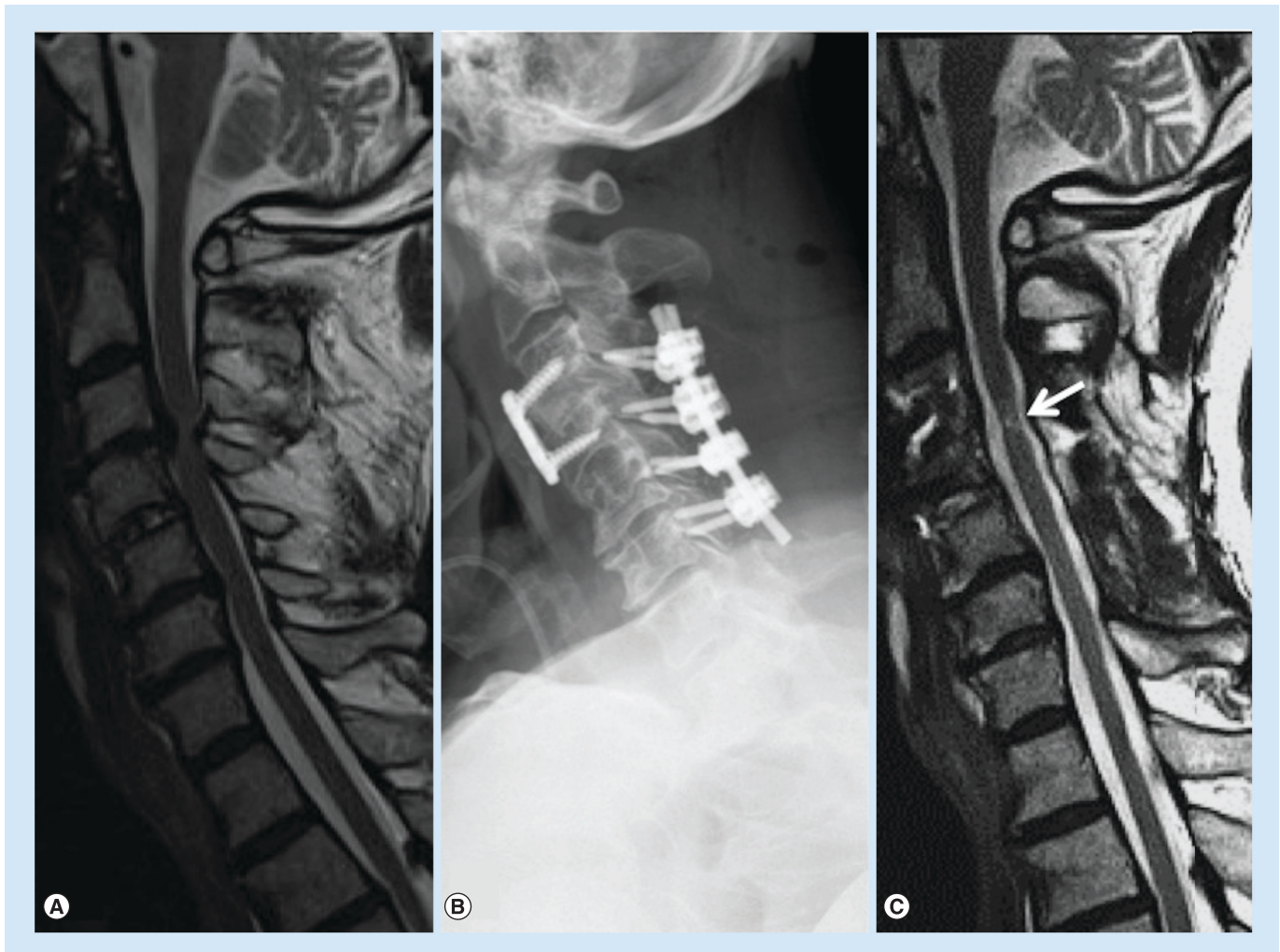


Figure 3. Postdecompression visibility of compressive myelopathy effects. (A) Sagittal T_2 preoperative image shows degenerative central canal stenosis and cord compression, with no clear high T_2 signal in the cord. (B) After surgical decompression, the (C) postoperative sagittal T_2 -weighted image shows a focus of myelomalacia in the cord (arrow) at the level of previous compression.

views: anteroposterior and lateral; additional views are generally required in specific conditions (e.g., open mouth for dens evaluation, flexion/extension for spine stability, and oblique views for peduncles or vertebral foramina assessment). Plain films evaluate the osseous structures and the vertebral alignment but, especially in situations where a SCC is suspected, have severe sensitivity limits, and from a first-line diagnostic imaging tool for spine-related conditions in the past, are nowadays progressively abandoned in favor of more advanced and accurate imaging modalities.

Multidetector CT

Multidetector CT (MDCT) is unparalleled in its capability to detect bone abnormalities, it ensures fast acquisition times, and is progressively widely available on the territory. With an isotropic volumetric acquisition, it guarantees high-quality thin-section multi-

planar reformatted images, with views for bone and soft tissues. Complex lesions can be more clearly depicted also using 3D capabilities of MDCT and, in the case of polytrauma patients, the images on the spine can be extracted from the data set of the patient's total-body CT [5,6]. MDCT can also depict significant soft tissue abnormalities (e.g., disk herniations, ligamentous degenerative hypertrophy, epidural lesions or collections; Figure 1) [7–10]. The most important limitation of this technique remains the inability to provide accurate information on spinal cord lesions and ligamentous injury. Clinicians and radiologists should also consider the significant radiation exposure of patients undergoing MDCT, and therefore, especially in the young population, limit this examination to necessary clinical indications, use available radiation-reduction tools and protocols, and generally apply the 'as low as reasonably achievable' imaging principles [11–13].

MRI

MRI is the best imaging modality to assess soft tissues, ligaments, disks and spinal cord. Any patient with presumed SCC should undergo a MRI examination as soon as possible to reveal the location and severity of spinal cord lesion [8,14–15]. High magnetic field apparatus (1.5–3.0 T) should be used to image the spinal cord. Accurate determination of intrinsic or extrinsic spinal cord lesions routinely requires the acquisition of two different pulse sequences, typically unenhanced T_1 - and T_2 -weighted images, in two orthogonal planes, usually axial and sagittal. Sagittal T_2 -weighted images are almost invariably acquired with fast spin echo (FSE) pulse sequences. Several T_2 -weighted pulse sequences are employed for axial imaging, FSE, gradient-recalled echo (GRE) and 3D constructive interference in the steady state myelographic images, each with specific advantages and limits. The images with the highest anatomical resolution, such as myelographic MRI suffer from intrinsic poor sensitivity for spinal cord parenchymal signal abnormalities; FSE images, with good sensitivity for spinal cord signal abnormalities are often disturbed by CSF flow artifacts, especially along

the ventral aspect of the spinal cord. GRE images are insensitive to flow artifacts, and provide good contrast between spinal cord and CSF, yet maintain good sensitivity for spinal cord parenchyma signal abnormalities, and are able to differentiate ‘hard’ calcified or ossified spondylotic spurs (hypointense) from ‘soft’ disc herniations (hyperintense), which may have importance for surgical decisions [16,17]. GRE T_2^* -weighted images, with an echo time of 20–25 ms are employed, in case of trauma, to detect hemorrhagic spinal cord injuries. Contrast-enhanced T_1 -weighted images can be necessary if a neoplastic, infectious, or inflammatory condition is suspected, clinically or on the basis of unenhanced images, or when imaging a postoperative spine [18]. The presence of adipose tissue in spinal osseous structures, epidural space, peri- and para-spinal soft tissues implies the need for rigorous fat-suppression techniques to be applied to T_2 -weighted and contrast-enhanced T_1 -weighted images [19]. Limits of MRI are the usual contraindications (i.e., pacemaker, metallic foreign bodies in particular locations or claustrophobia), the length of scan, the absolute need for cooperation or of sedation/general anesthesia otherwise,

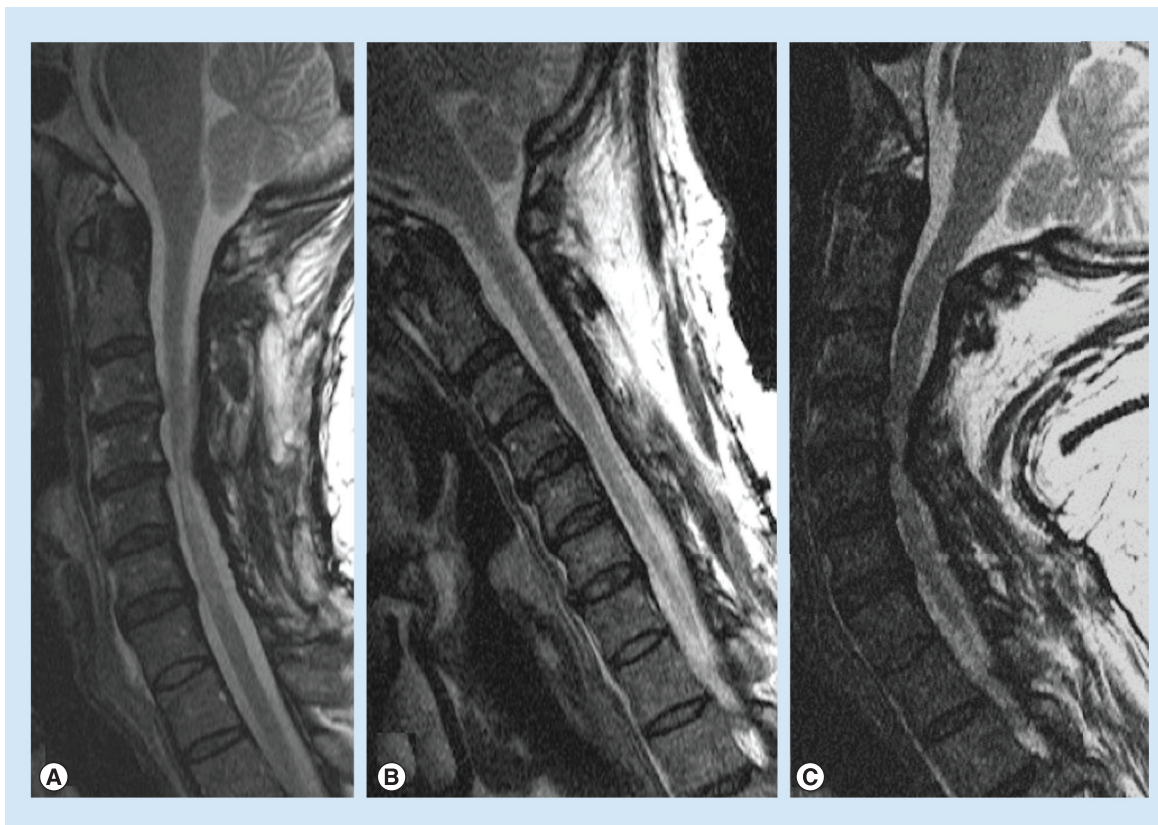


Figure 4. Degenerative cervical spinal cord compression unmasked by dynamic flexion–extension MRI. (A) Neutral sagittal turbo spin echo T_2 -weighted image shows myelomalacia and cord atrophy, with no clear significant cord compression. Dynamic plain films (not shown) revealed no obvious instability. (B) Flexion and (C) extension MRI unmask an obvious severe multilevel degenerative central canal stenosis and cord compression in the extension posture.

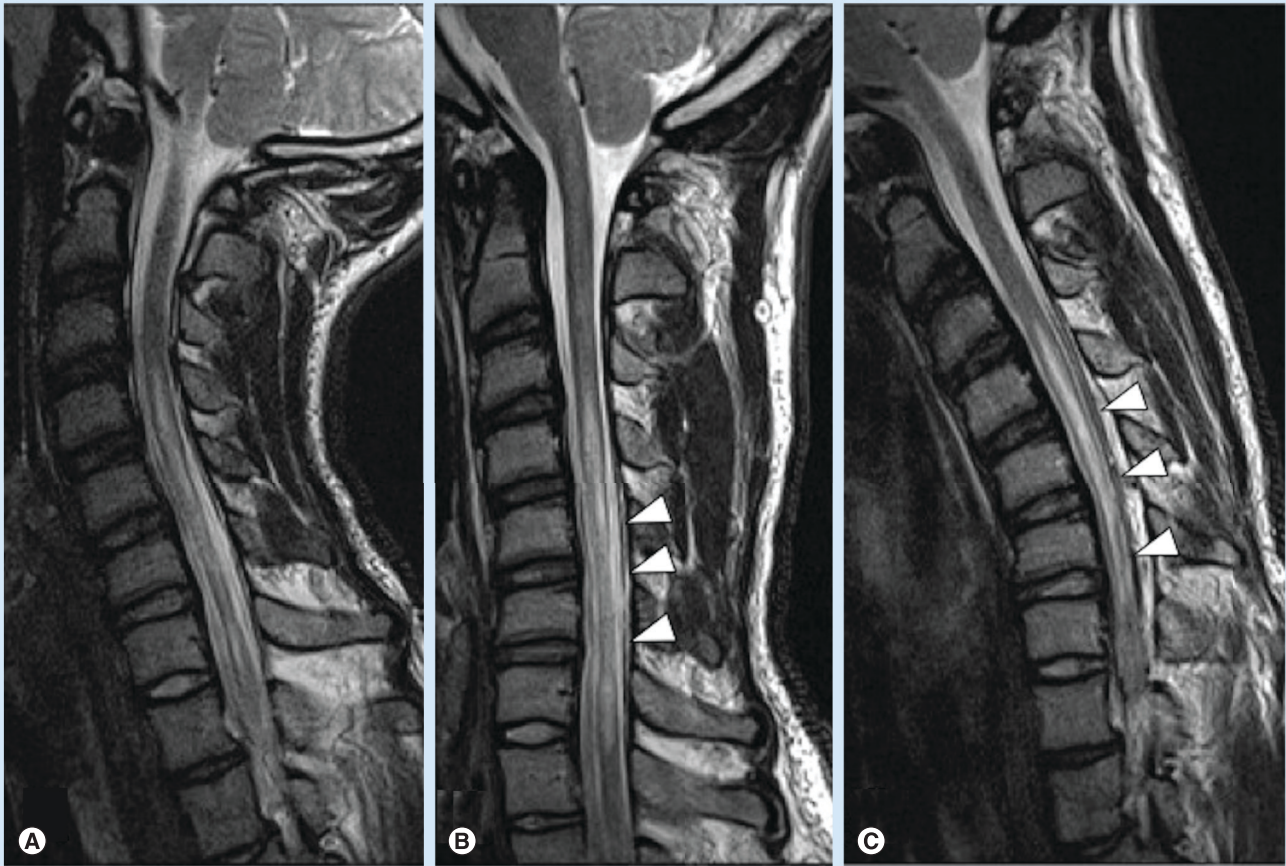


Figure 5. Hirayama flexion myelopathy. (A) In this patient with myelopathy, clinical signs worsening in neck flexion, with unremarkable dynamic plain films (not shown), sagittal T_2 -weighted image in neutral position reveals extensive signs of chronic myelopathy, without definite cord compression. (B & C) In two different degrees of neck flexion, there is evidence of a progressive ventral shift of the hypointense thin dural lining (arrowheads), causing effacement of the subarachnoid space and compression of the cord. The loss of attachment and ventral displacement of the dura is a diagnostic feature of Hirayama disease.

the difficulty to control vital parameters in critically ill patients, and the relative limited availability of MRI, especially in the emergency situations.

What do we look for on MRI?

The presence of SCC needs to be distinguished from noncompressive spinal cord abnormalities. Therefore, we look for masses or other pathological processes that exert extrinsic mass effect on the spinal cord. In a normal condition, the spinal cord is circumferentially surrounded by CSF, which offers a high contrast background for the visualization of the cord on T_2 -weighted images. Sagittal T_2 -weighted images usually offer the most panoramic overview of the spinal segment in examination. This set of images offers immediate evidence of the vertebral body alignment, the CSF surrounding the spinal cord, the morphology, course, size and signal of the spinal cord, and the presence of

masses or collections compressing it. If a mass causing dislocation, deformation or compression of the cord is noted, attention to the presence of high T_2 signal abnormality is necessary. Notably the presence of an ill-defined high T_2 signal and swelling of the spinal cord parenchyma above and below the compression can suggest the presence of edema, suggesting acute compressive myelopathy (Supplementary Figure 1; see online at www.futuremedicine.com/doi/suppl.iim.13.71). Studies in animals [20,21] have shown that acute anterior SCC results in stenosis and occlusion of the epidural venous plexus, which causes breakdown of the blood–spinal cord barrier and results in vasogenic edema. The venous outflow impairment is more severe when compression occurs at two adjacent levels. Subsequently, compression causes impairment of arterial blood flow with cord ischemia and irreversible changes. In this chronic, terminal stage, MRI show a more well-defined high signal

on T₂-weighted images, with volume loss indicative of gliosis and myelomalacia (Figure 2). Despite the high sensitivity of sagittal T₂-weighted images, axial T₂-weighted images are necessary to confirm the spinal cord signal abnormality, the true degree of a SCC and the severity of central canal stenosis (Figure 2B & 2C). It should be noted that in a severely compressed spinal cord, high T₂ signal edema may not be visible at the level of maximum compression, but be evident cranially and caudally in the cord. In such cases, edema may become clearly evident once decompression of the cord is achieved, thereby displaying the MRI signs of compressive myelopathy (Figure 3). Contrast-enhanced images are not necessary in the trauma setting, but usually acquired when an infectious or neoplastic process is suspected. In the setting of SCC, on T₁-weighted postcontrast images, a dilated and congested enhancing epidural venous plexus can be noted above and below the compressed level, more frequently in the ventral epidural space, but sometimes circumferentially; this represents a potential pitfall, mimicking abnormal enhancing epidural tissue or phlegmon.

In selected cases, to unmask a condition of clinically suspected cervical SCC, but with no clear evidence at

standard MRI, MRI with neck flexion and extension can reveal dynamic stenosis (Figure 4) or Hirayama flexion myelopathy (Figure 5) [22,23].

Advanced MRI techniques: future perspective

Standard morphological T₁- and T₂-weighted images are not always accurate in grading the severity of the myelopathy, and the degree of SCC does not always correlate with clinical severity. Recent technological advances (e.g., diffusion-weighted imaging [DWI], diffusion tensor imaging [DTI] and tractography) have recently been applied to the study of the spinal cord, with the intent to characterize neural tissue at a microstructural level (Figure 6) [24]. Future applications of these techniques that actually are not routinely performed in the clinical ground, may be the assessment of the functional integrity of the axons within the white matter tracts of the compressed spinal cord, and the prognostic prediction upon its treatment [25–28].

Myelo-CT

Myelo-CT is reserved to selected cases when MRI is not feasible or results are unclear, and can render

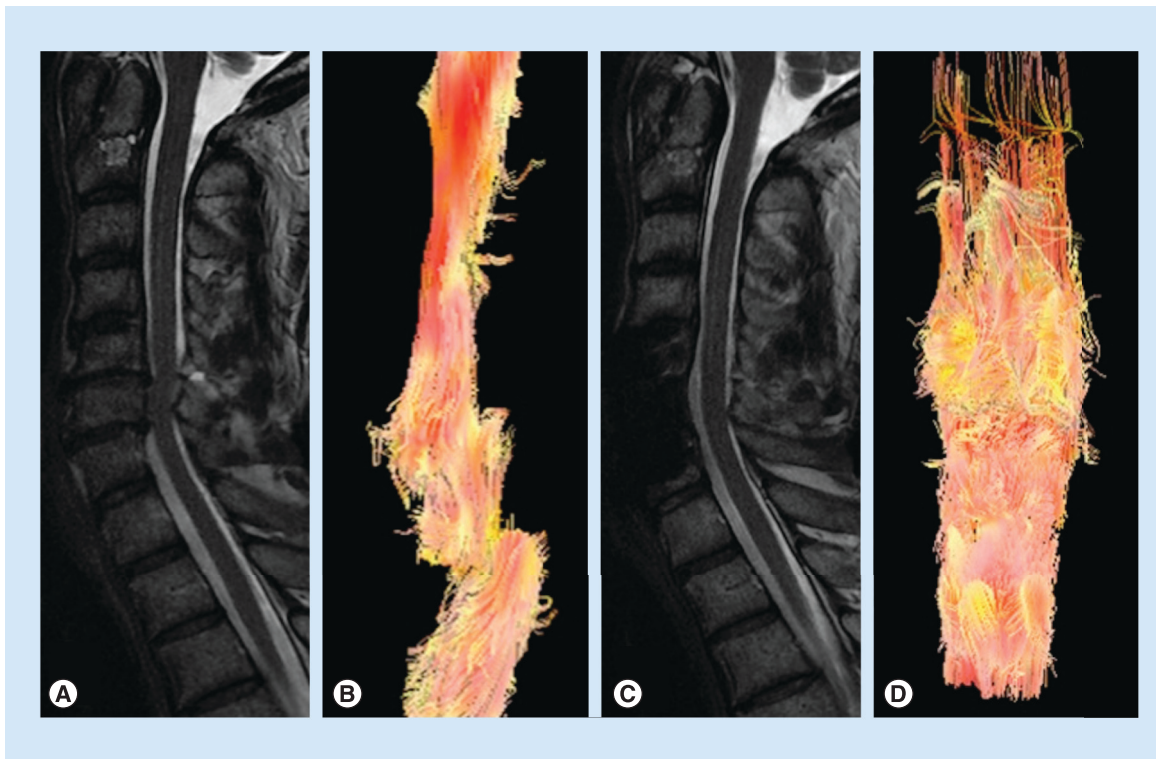


Figure 6. Diffusion tensor tractography. Diffusion tensor imaging can be performed on the spinal cord where it reveals microstructural arrangements of white matter fibers. In this case of degenerative cervical central canal stenosis and moderate cord compression, (A) MRI sagittal T₂-weighted imaging does not reveal a definite signal abnormality in the cord, but (B) tractography shows abnormal arrangement and loss of continuity of the cord's white matter fibers. (C & D) The control postsurgical decompression reveals reconstitution of normal white matter tracts. Images courtesy of Dr Meng Law, USC Keck Medical Center (CA, USA).

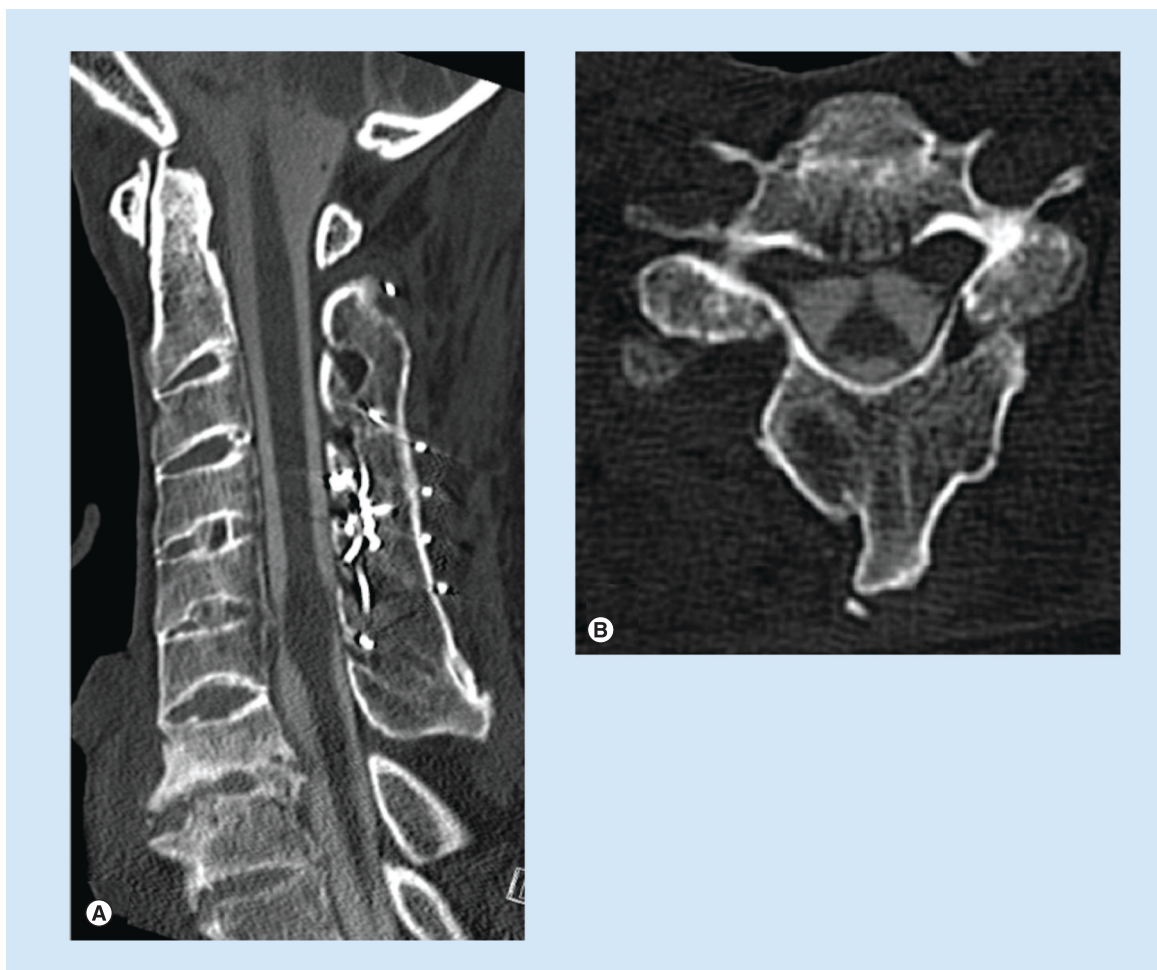


Figure 7. CT myelography. In this patient with worsening cervical myelopathy after surgical decompression and fusion, MRI (not shown) revealed signs of spinal cord tumefaction, but image quality was poor due to metallic artifacts caused by wires in the posterior fusion mass. (A) CT myelography sagittal and (B) axial images show, with high spatial and contrast resolution, the deformed aspect of the cord, caused by meningeal adhesions (arrows in B), sign of postsurgical arachnoiditis. No information are provided by these images on the presence of cord edema or other myelopathic changes.

additional information compared with MDCT, with an accurate visualization of the intradural extramedullary compartment (Figure 7) [29]. Myelo-CT is less sensitive than MRI to metallic artifacts, especially in the case of implanted hardware, is not affected by flow artifacts, and offers high contrast and spatial resolution, but owing to complete lack of sensitivity in detecting intrinsic spinal cord abnormalities, can only partially replace MRI. In addition to its diagnostic limits, myelo-CT suffers from a series of disadvantages versus MRI, such as invasiveness of lumbar puncture and intrathecal contrast agent injection, ionizing radiation exposition, need of mobilization of the patient to allow for injected contrast to diffuse from the point of injection to the spine level of interest and the need of injection of contrast from below and above the compression level in case of myelographic block.

How to image the patient with SCC: diagnostic pathways

The SCC radiological work-up is generally designed upon the clinical setting. There is a general consensus that spine trauma patients need to be evaluated by emergency MDCT to assess presence of luxations or fractures [30,31]. While a negative MDCT exam is believed to be able to virtually rule out an unstable spine lesion by itself [32,33], patients with neurological symptoms, especially those suggesting SCC, absolutely need diagnostic complement by an emergency MRI, regardless of the positive or negative results of MDCT [34–38]. In all other nontraumatic spinal cord syndromes, in which SCC needs to be ruled out, with an acute, subacute or chronic presentation, MRI can be considered as first-line imaging method. MDCT should be considered as a complementary exam to further characterize osseous abnormalities revealed by MRI. Myelo-CT might be

Table 1. Spinal cord compression: site of origin for differential diagnosis.

From osseous compartment	From epidural space	From intradural space
Fractures with posterior wall retropulsion/ facet dislocations	Epidural abscess	Primary neoplasm and metastasis
Metastasis and osseous spine tumor	Epidural hematoma	Subdural hematoma
Aggressive hemangioma	Disc herniation	Arachnoid cyst
Degenerative disease	Synovial cyst	–

useful in selected cases, when MRI is not possible or of unsatisfactory diagnostic quality, due to motion or metallic hardware artifacts, or when there is a poor correlation between symptoms and MRI, especially in the chronic degenerative setting [4].

Lesion's site of origin

SCC may be caused by different pathologies arising from or involving different anatomical compartments. The differential diagnosis is strictly influenced by the recognition of the lesions's compartment of origin. Once the anatomic site of lesion's origin has been determined, a narrowed differential diagnosis requires consideration of both clinical and specific imaging data.

Table 1 shows an anatomically based differential diagnosis of the most common causes of SCC, depending on the site of origin of the lesion causing SCC.

To evaluate the complexity of SCC in a logical concise manner, we suggest to schematically divide the spinal environment into osseous, epidural and intradural compartments.

In the osseous compartment, we include the osseous spinal column, the discs and the spinal ligaments, bordering the central canal and the neuroforamina.

The epidural compartment is contained between the inner aspect of the bony central canal and the dura mater. Differently from the intracranial compartment, in the spine, the dura mater is not attached to the bone, therefore the epidural space is not virtual but a real space, and contains adipose tissue and a rich vascular network, forming the epidural venous plexus, which is more largely represented in the ventral epidural space. The intradural extramedullary compartment is outlined by the dura mater, and

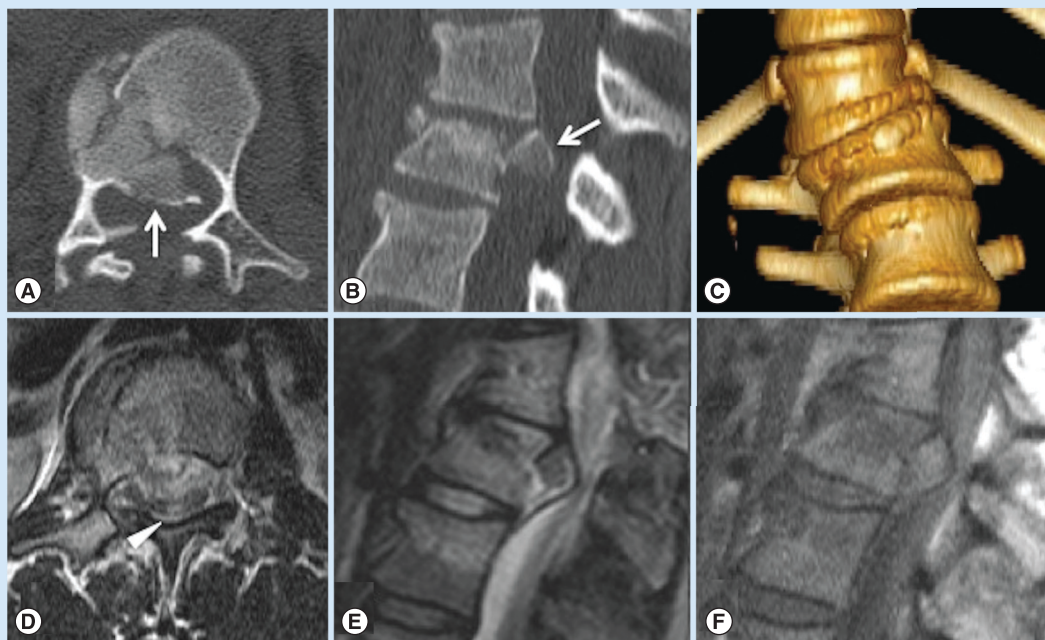


Figure 8. Burst fracture. (A) Axial, (B) sagittal reformatted and (C) 3D volume rendering CT images demonstrate the vertebral fracture due to high energy axial load compression force. The vertebral body shows comminution and outward displacement of fragments; the posterior wall is retropulsed and occupies the central canal (arrow in A & B). (D) Axial and (E) sagittal turbo spin echo T₂-weighted and (F) T₁-weighted images allow visualization of soft tissue and neural structures; the spinal cord is severely compressed, with focal high T₂ signal suggestive of edema (arrowhead in D).

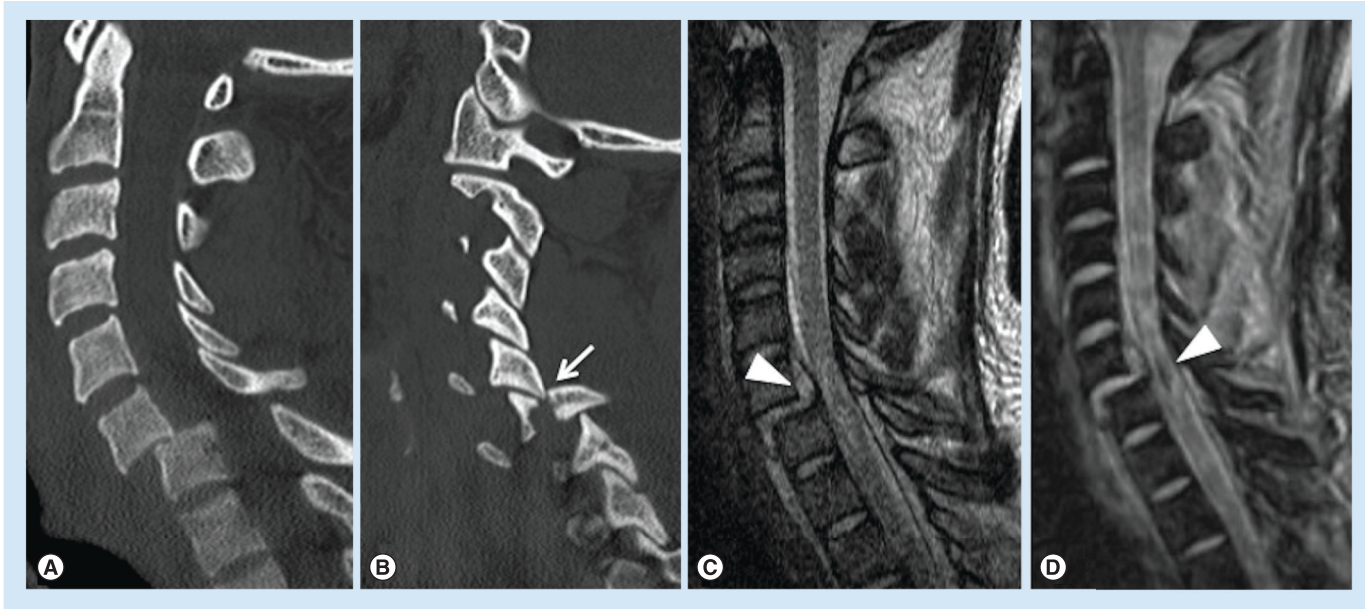


Figure 9. Fracture luxation. (A & B) Sagittal reformatted multidetector CT images show facet fracture and dislocation (arrow in B) causing severe anterior spondylolisthesis and canal narrowing. After joint dislocation reduction, (C) MRI with sagittal T₂-weighted turbo spin echo and (D) T₂*-weighted gradient-recalled echo is obtained, showing satisfactory partial realignment, but also depicts other crucial findings: a large disk herniation caused by extensive disco–ligamentous complex injury, is still compressing the cord (arrowhead on C), and the cord shows signs of edema and low signal hemorrhage (arrowhead on D).

includes the subdural and the subarachnoid spaces. While the subdural is a virtual space, between dura and arachnoid, the subarachnoid space is filled with CSF and contains leptomeninges, nerve roots, and arterial and venous intradural spinal vessels.

Finally the intradural intramedullary compartment represents the spinal cord itself, bordered by the pia mater.

**Cause of SCC from the osseous compartment
Traumatic fractures & dislocations**

Following a vertebral fracture or dislocation, an osseous fragment can violate the central canal and impinge on the spinal cord, or an entire vertebra can shift axially, disrupt and narrow the integrity of the central canal.

Axial load burst fractures, flexion tear-drop fractures and fractures–dislocations are the most common

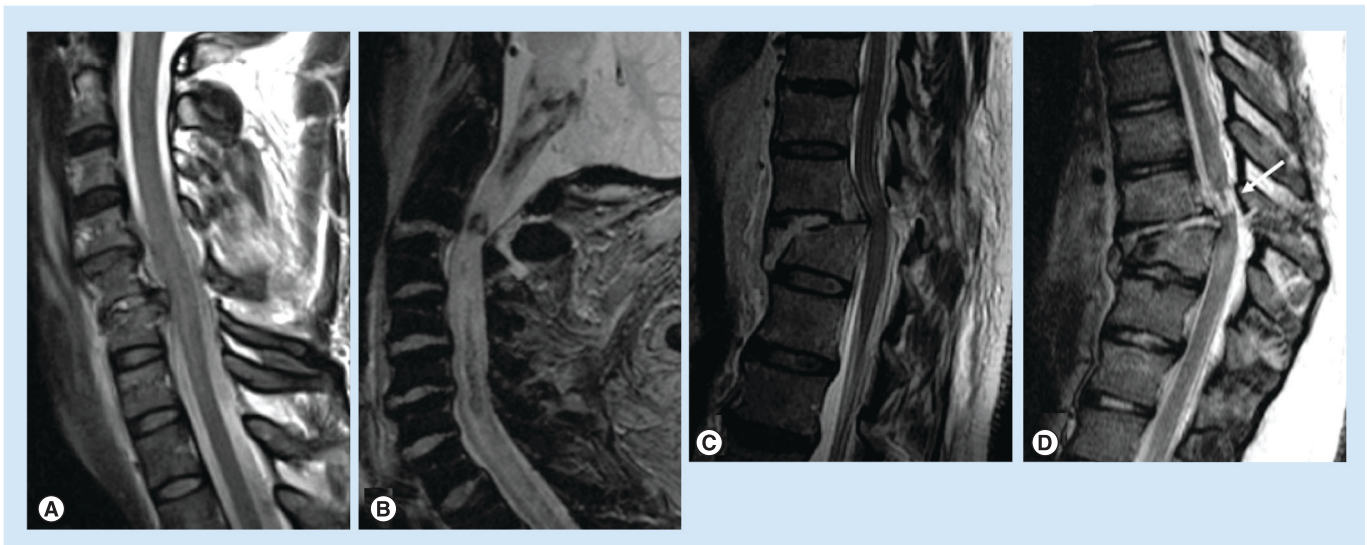


Figure 10. Traumatic cord injury. Four different examples of traumatic cord injuries of different severity. (A) Edematous nonhemorrhagic cord contusion revealed by high T₂ signal and cord swelling. (B) Hemorrhagic cord contusion revealed by low T₂* signal on gradient-recalled echo T₂*-weighted image. (C) Cord compression, with a deformed, angulated, edematous, but apparently intact cord. (D) Complete cord transection, as revealed by a cerebrospinal fluid-like signal gap in the cord at the level of fracture–dislocation and kyphosis (arrow).

traumatic causes of SCC with different underlying mechanism of injury.

Burst fractures consist of a vertically oriented fracture of the vertebral body with lateral dispersion of the fracture fragments: the posterior wall of the vertebral body is disrupted, the distance between the pedicles is widened, and there are associated fractures in the posterior elements. With burst fractures, the energy from the axial load is transferred to the vertebral bodies and intervertebral discs and consequently to neurologic structures, that experience the kinetic energy from the retropulsed vertebral bone fragments. MDCT allows an accurate and clear demonstration of the degree of vertebral comminution, as well as canal compromise by the retropulsed bony fragment (Figure 8) [39]. MRI allows visualization of

neural structures and soft tissues [40], detects spinal cord lesions, disk herniations and epidural hematomas (EDHs), possibly contributing to the cord compression.

Flexion teardrop fractures are due to hyperflexion forces of great magnitude that cause a wedge deformity and a fracture of a large triangular portion of the antero-inferior portion of the vertebral body, associated with posterior ligament disruption. This type of spinal injury is usually complicated by middle columns fractures and retropulsion of bony fragments into the spinal canal (Supplementary Figure 2).

Fractures/dislocations consist of different degrees of anterior luxation of the upper vertebra above the lower vertebra consequent to uni- or bi-lateral facet dislocations associated with facet capsules, posterior

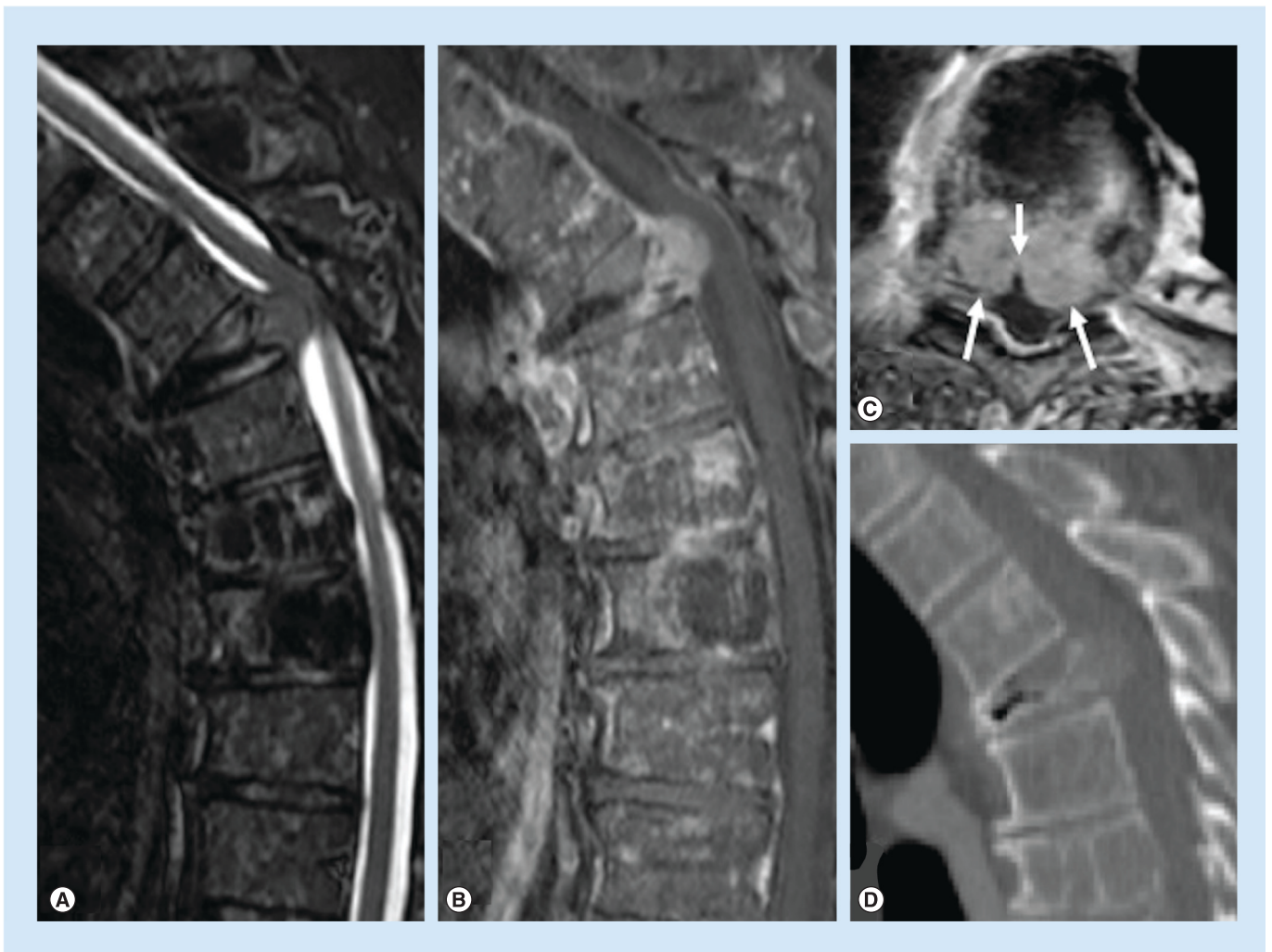


Figure 11. Pathologic fracture with spinal cord compression. (A) Sagittal short tau inversion recovery image reveals a collapsed vertebral body with a large epidural mass compressing the spinal cord; (B) sagittal and (C) axial contrast-enhanced fat-suppressed turbo spin echo T_1 -weighted images highlight the neoplastic tissue that involves the anterior epidural space. Axial image depicts the 'draw-curtain sign' (arrows), a sign indicative of neoplastic epidural involvement. (D) Sagittal reformatted CT image demonstrates the lytic pattern of neoplastic growth also at other vertebral levels.

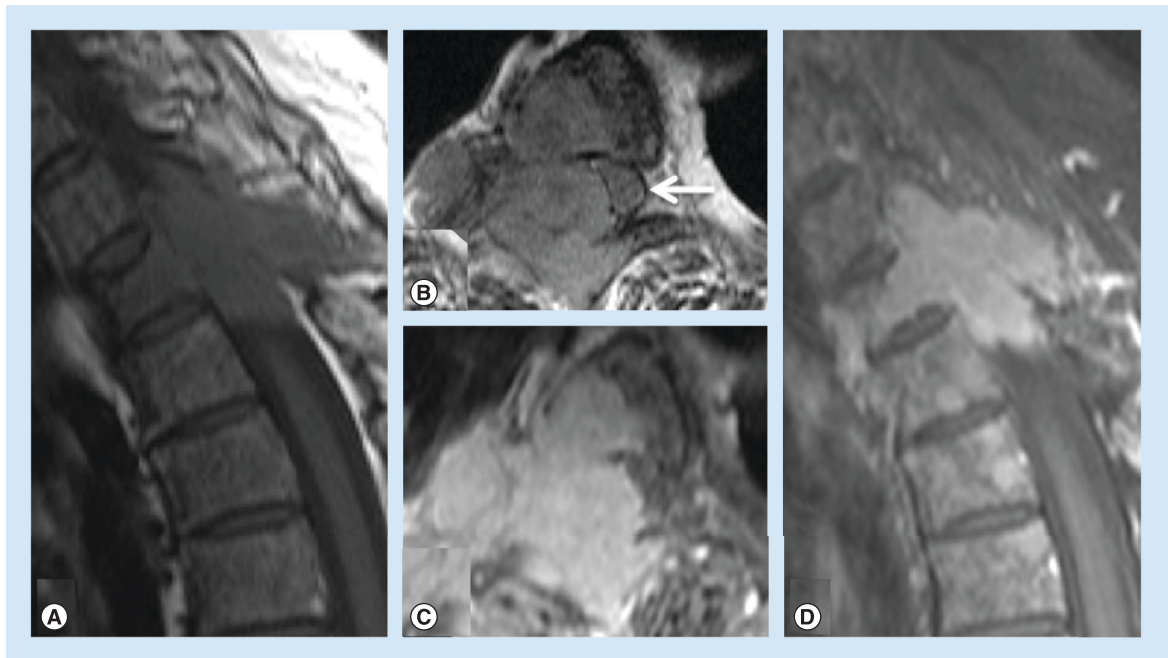


Figure 12. Spinal cord compression from vertebral tumor. Extensive myelomatous bony involvement with endocanalicular epidural extension: (A) the mass is hypointense on the turbo spin echo T_1 -weighted image, (B) slightly hyperintense on T_2 -weighted image, with (C & D) intense and homogeneous enhancement on postcontrast fat suppressed images. The spinal cord is laterally displaced (arrow in B) and moderately compressed.

longitudinal ligament, annulus fibrosus, and interlaminar and interspinous ligament disruption (Figure 9). The spinal cord compromise results from kyphotic and translation deformities with shearing and stretching injuries [41]. MRI plays a fundamental role in the assessment of traumatic cord injury showing a large spectrum of abnormalities, such as cord

compression, cord edema, hemorrhagic contusion and transection (Figure 10). Cord edema is detected as high T_2 signal and normal–low T_1 signal within the cord, with a variable grade of swelling [42]. Cord edema is not static and changes significantly within the first 2 weeks following injury; it can gradually resolve or it can evolve in a progressive ascend-

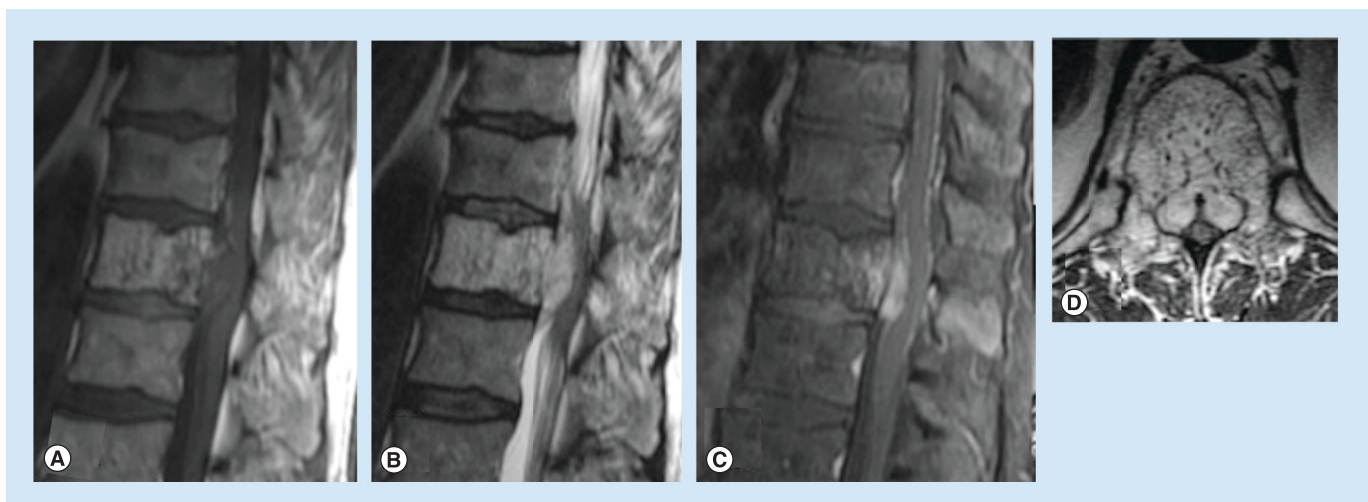


Figure 13. Vertebral hemangioma with extra-osseous extension. (A) Sagittal turbo spin echo T_1 -weighted and (B) T_2 -weighted images show typical MRI features of T_1 - and T_2 -hyperintense locally aggressive vertebral hemangioma extending into the spinal canal causing compression of the spinal cord. The vertebral body component shows minimal enhancement, while the epidural mass shows contrast enhancement, as depicted on (C) fat-suppressed enhanced T_1 -weighted image. (D) Axial T_2 -weighted image depicts typical 'draw-curtain' sign and stippled appearance of the vertebral body, representing thickened osseous trabeculae; the cord appears compressed and posteriorly displaced.

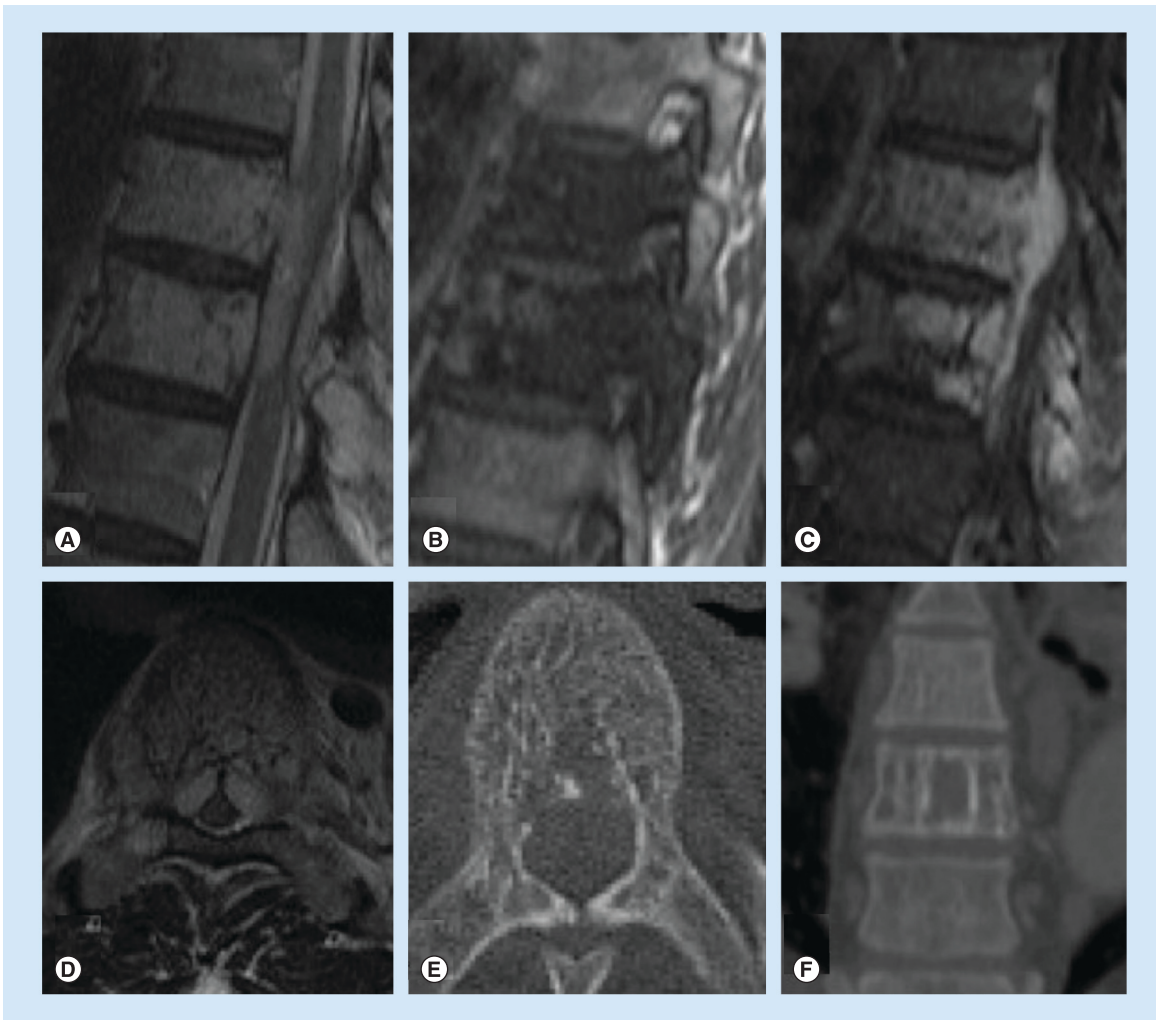


Figure 14. Aggressive vertebral hemangioma with atypical MRI features. The lesion involves two adjacent thoracic vertebral levels that appear hyperintense on (A & D) turbo spin echo T_2 -weighted images, but hypointense on (B) T_1 -weighted image, with intense but somewhat inhomogeneous contrast enhancement on (C) enhanced fat-suppressed T_1 -weighted image. (D) The neoplasm extends into the epidural space compressing the spinal cord. (E) Axial and (F) coronal reformatted CT images show the typical coarse and thickened appearance of the osseous trabeculae, spaced by large vascular spaces.

ing myelopathy [43]. In some cases the swollen and enlarged cord appears compressed in a central canal that would otherwise be of normal width; surgical decompression in such instances should be considered to reduce the risk of vascular cord compromise and further spinal cord damage [44]. The presence of hemorrhage within the cord (hemorrhagic contusion) has been associated with unfavorable prognostic outcome [34,45]. In these cases, a GRE T_2^* -weighted sequence, which we suggest to acquire in the sagittal plane, should be used and may reveal foci of signal loss indicative of presence of blood products (Figure 10B). Cord transection is the most severe cord injury characterized by loss of continuity of the cord, with a CSF or blood-filled gap indicative of complete disruption of the cord (Figure 10D).

Osteoporotic fractures

Insufficiency fractures, spontaneous or precipitated by minor trauma, are usually characterized by wedge, concave, biconcave or crush deformity. These are often subclinical, and when occurring at multiple levels can result in spinal deformity, but are almost invariably stable fractures. When posterior wall involvement is seen, this is typically seen at its superior corner, that can be retropulsed and impinge upon the central canal. Since this morphology of the fracture occurs more frequently at the lumbar level, when the retropulsion is significant, it is more frequently cause of radiculopathy [46].

Pathologic fractures

Neoplastic overgrowth inside the vertebra may be responsible for destruction of osseous architecture and

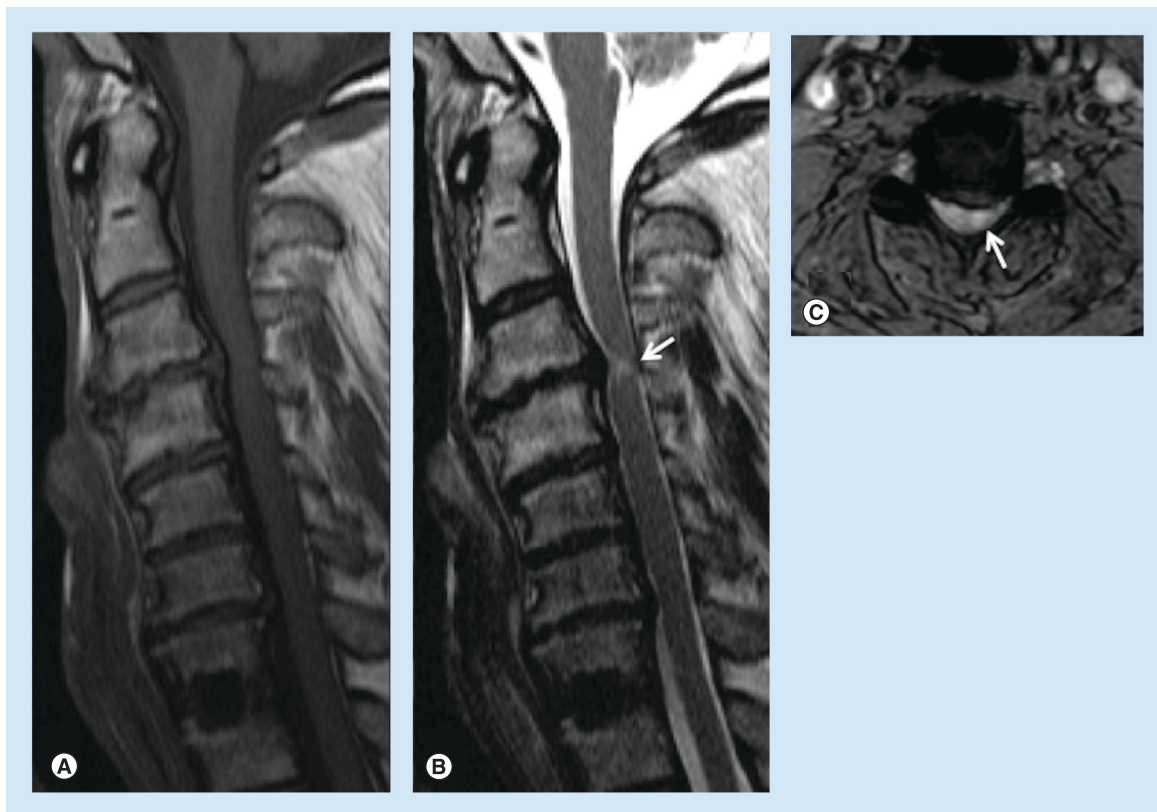


Figure 15. Chronic compressive myelopathy. (A) Sagittal turbo spin echo T_1 -weighted and (B) T_2 -weighted images show severe cervical spondylotic changes with central canal stenosis at C3–C4. The cord is compressed and displays a focal well defined area of high T_2 signal (arrow on B), which is confirmed in the left side of the cord by (C) the axial gradient-recalled echo T_2 -weighted image (arrow on C). This focal cord lesion with sharp borders is supposed to represent an area of chronic gliosis and myelomalacia.

weakening of the vertebral body. This may result in an insufficiency fracture, but differently from an osteoporotic fracture, the neoplastic soft tissue invading the vertebral body can be displaced posteriorly in the central canal, and more frequently causes SCC. While signal abnormality or contrast-enhancement of the vertebral body cannot reliably distinguish a recent osteoporotic from a malignant fracture, the convex aspect of the posterior wall, a soft tissue epidural mass on MRI, a frankly lytic lesions on CT, or more rarely sclerotic changes, are rather specific signs, when present, of a pathologic fracture (Figure 11 & Supplementary Figure 3) [47].

Vertebral neoplasms

Tumors arising from the vertebral osseous structures can cause SCC, even in the absence of a pathologic fracture, in the case of extra-osseous neoplastic overgrowth and invasion of the epidural space. Multiple myeloma and osseous metastasis from solid tumors represent the most common causes of SCC from osseous spine tumors [48]. MRI usually shows a low T_1 signal, a high T_2 signal and contrast enhancement in the affected bone and in the epidural mass (Figure 12 & Supplementary Figure 4) [49].

It should be noted that nonfat-suppressed T_2 -weighted and enhanced T_1 -weighted images have low sensitivity for neoplastic osseous lesions, due to the confounding effect of an intrinsically high T_1 and T_2 signal of the normal yellow bone marrow. Fat-suppressed axial T_2 and enhanced T_1 images, with fat saturation, depict the extent of involvement of the epidural space, the degree of SCC versus dislocation and the presence of an abnormal T_2 signal in the cord, the imaging hallmark of compressive myelopathy (Supplementary Figure 5). Neoplastic epidural spread more frequently than other non-neoplastic pathological conditions in this location, such as epidural abscess or hematoma, shows the bilobed or unilobed appearance, or ‘drawn-curtain’ sign, of abnormal tissue within the ventral epidural space (Figure 11 & Supplementary Figure 5) [50]. The pattern of enhancement may be an additional helpful sign to differentiate neoplastic disease that generally shows solid enhancement, abscesses that show peripheral enhancement and central fluid components, and hematomas that generally do not enhance, especially in the early stage [19]. The panoramic features of MRI can frequently depict multiple vertebral localizations,

which further direct the diagnosis toward a neoplastic etiology. Clinical information and patient's history are obviously essential data to reduce the spectrum of differential diagnosis.

Nonenhanced CT with a bone reconstruction algorithm is extremely helpful in defining both lytic and blastic lesions and in visualizing the presence of cortical destruction.

Aggressive hemangioma

Vertebral hemangioma is a postcapillary cavernous vascular malformation, usually characterized by extremely slow flow, which may expand the periosteum and extend into the soft tissues. Vertebral hemangioma may be symptomatic when progressive spinal cord or nerve–root compression occurs due

to growth of the lesion beyond the confines of the vertebral body, or because of compression fracture or epidural hemorrhage [51]. MRI can show the typical hyperintense T_1 and T_2 signal (Figure 13). Presence of highly vascular or fibrotic components may render imaging characteristics atypical, with a low T_1 signal (Figure 14), posing a more difficult differential diagnosis with a neoplastic lesion. Contrast-enhancement of such lesions is variable, can be intense or inhomogeneous (Figures 13 & 14). CT in such cases might be useful depicting the coarse and stippled appearance of the osseous trabeculae of the vertebral body and the bony expansion and remodeling (Figure 14). MRI is the method of choice to depict the extent to the posterior elements, to the epidural space, and the SCC [52].

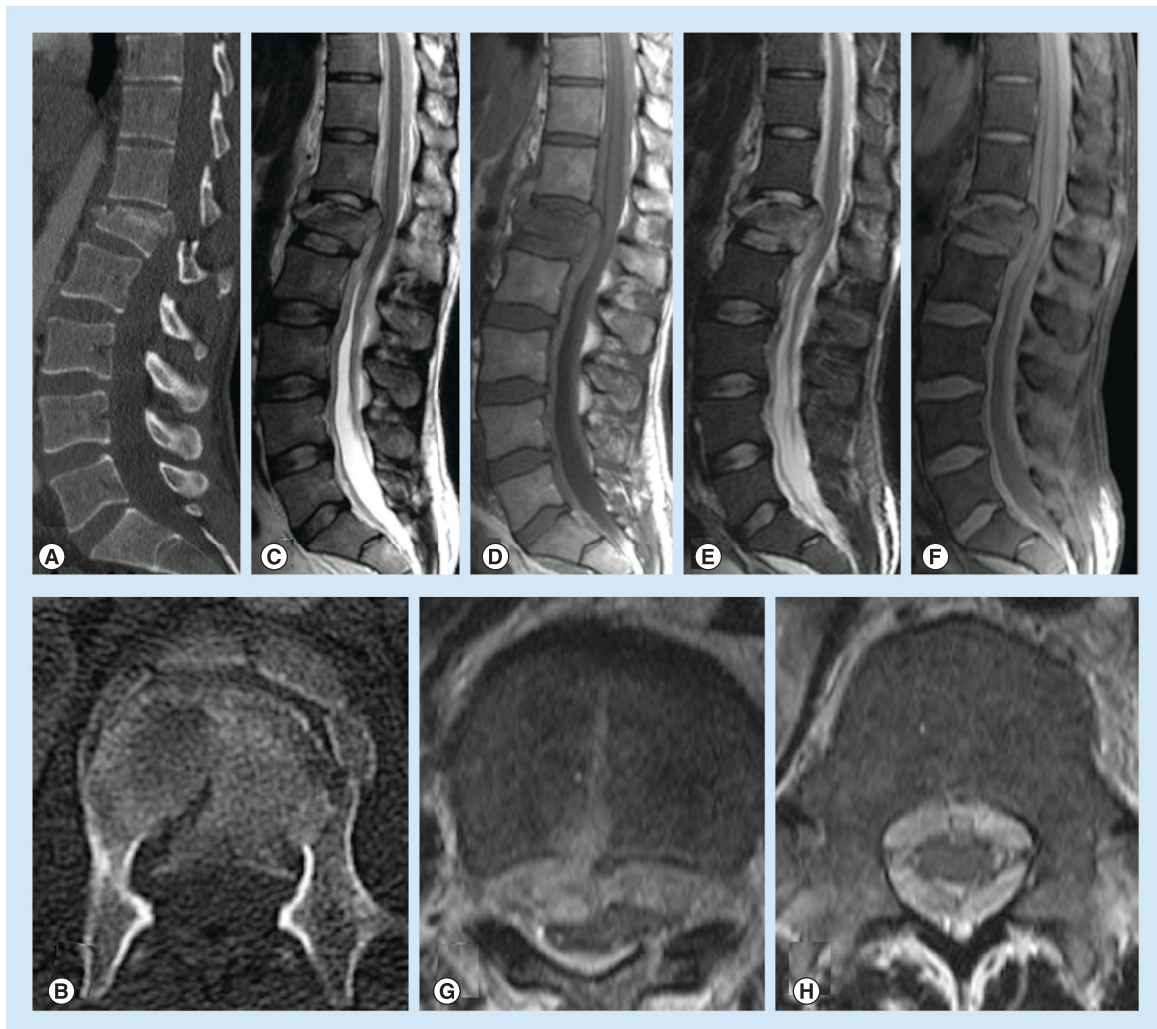


Figure 16. Epidural hematoma. (A & B) Sagittal reformatted and axial CT images show a L1 burst fracture with posterior wall retropulsion. (C) Sagittal turbo spin echo images evidence an extensive epidural collection hyperintense to the spinal cord on T_2 -weighted and (D) T_1 -weighted images. The collection appears more relatively hyperintense on fat-suppressed (E) T_2 -weighted and (F) T_1 -weighted images. (G & H) Axial turbo spin echo T_2 -weighted images evidence the severe mass effect on the spinal cord caused by the fractured posterior wall and the circumferential epidural hematoma.

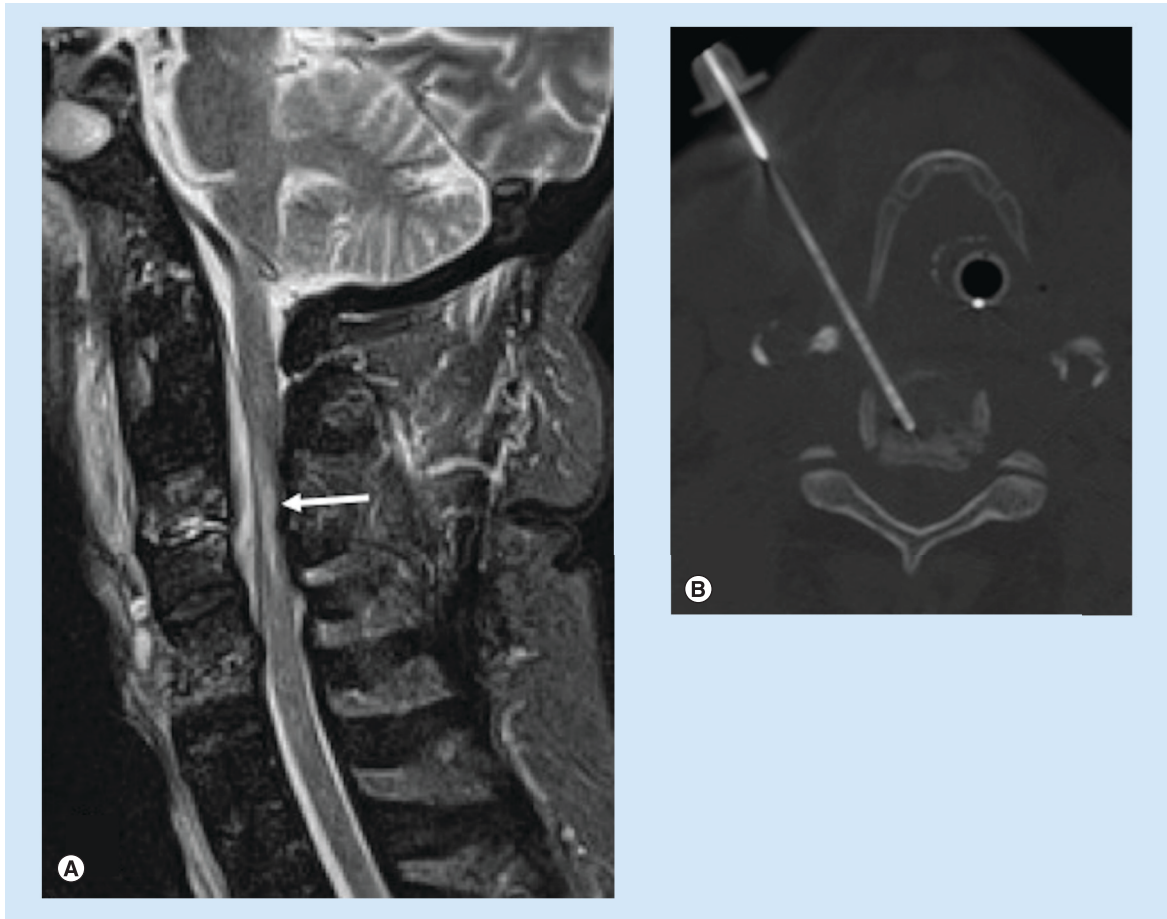


Figure 17. Epidural abscess with spinal cord compression. (A) Sagittal fat-suppressed turbo spin echo T_2 -weighted image shows two possible foci of spondylodiscitis, at C3–C4 and C5–C6, with prevertebral soft tissues thickening and edema, likely a phlegmon, and a ventral epidural fluid collection from C2 to C5 compressing the spinal cord, likely an abscess. No contrast agent was injected due to renal insufficiency. The spinal cord shows high T_2 signal (arrow on A) suggesting edema and myelopathy. (B) shows the CT-guided C3–C4 disc aspiration, which retrieved purulent fluid, probably also partially draining the abscess. Microbiology analysis revealed *Staphylococcus aureus*.

Degenerative osseous & nonosseous causes of SCC

Vertebral posterior osteophytes, disc-osteophyte complexes, ligamentous calcification and ossification, articular masses hypertrophy, and degenerative antero- and retro-listhesis are the most common cause of spinal stenosis, nerve root compression and compressive changes of the spinal cord, especially in the cervical region. These spondylotic changes, present with high prevalence in the elderly population, with different degrees of severity and with variable clinical expression, can be responsible of neurological symptoms that develop slowly, over months to years, generally related to vascular compromise of neural tissue. An accurate imaging diagnosis, and strict clinical correlation are important to guide treatment and to predict prognosis. MRI is the most commonly used tool for delineating the extent of the degenerative changes, the degree of narrowing of the spinal canal and the spinal cord alterations, second-

ary to edema, ischemia or myelomalacia. A standard imaging protocol for such conditions include sagittal T_2 - and T_1 -weighted sequences, completed with an axial T_2 -weighted set of images. CT can be of complementary use to precisely depict the anatomy of calcific and osseous structures, measuring precise diameters of central and foramina bony canals. Plain films, usually performed with dynamic views, can provide valuable information (e.g., spine stability) to guide treatment. CT myelography is used when MRI is not feasible, or results are incongruent with clinical data.

Typical MRI findings of compressive myelopathy is an intramedullary high signal on T_2 -weighted images at the level of cord compression, which can be fuzzy and vague, or intensely bright and well defined (Figure 15 & Supplementary Figure 1) [53,54]. It has been reported that high signal intensity of the spinal cord reflects pathological changes, both reversible and irreversible. Increased T_2 signal intensity in the

spinal cord usually corresponds to water content or occasionally to the presence of blood or serum [55–58]. In a cadaveric study, Ohshio *et al.* [59] related high signal intensity on T₂-weighted images of the cord to histologic changes, such as gliosis, edema, necrosis, myelomalacia or spongiform changes in the gray matter with edema, Wallerian degeneration, demyelination and necrosis of the white matter. There is controversy about the prognostic role of high signal intensity on T₂-weighted images: several authors have reported intramedullary high signal as a sign of poor prognosis, while others reported no correlation with prognosis [60–62]. A study [60] found that a predominantly well-defined area of intramedullary high signal intensity on T₂-weighted has a poor prognostic meaning towards recovery after surgical decompression, whereas patients with predominantly ‘faint and fuzzy’ borders area of intramedullary high signal intensity have the same outcome as those without signal intensity changes. Another study reported that patients with multisegmental areas of high T₂ signal intensity have a poorer prognosis than patients with unisegmental areas of abnormal signal intensity [63]. Intramedullary contrast enhancement in compressive myelopathy has also been described [64,65], and some authors have reported a negative prognostic factor for recovery in patients undergoing decompressive surgery (Supplementary Figure 6) [66].

The most recent consensus seem to point to a rather poor specificity of conventional MRI findings, such as a high T₂ signal in the cord, in discriminating potentially reversible edema and ischemia from irreversible myelomalacia and gliosis; several researches on DWI and DTI on spinal cord have been carried out in the past few years and have showed superior correlation of DWI and DTI measurements with clinical and electrophysiological signs of myelopathy, compared with conventional MRI [67–72]. Similarly, fractional anisotropy measurements seem to be able to predict recovery upon surgical decompression [28]. Nevertheless, these techniques have not yet been implemented in routine imaging, and require further research.

Spinal cord injury without radiographic abnormality

Spinal cord injury without radiographic abnormality is defined as the presence of spinal cord injury in the absence of a fracture or dislocation on plain radiography or CT scan. An MRI rules out SCC in the patient with neurological deficit following spinal trauma. Spinal cord injury without radiographic abnormality is usually due to contusion or cord stretching. It occurs in the pediatric population, as a consequence of children’s vertebral column elasticity and vulnerability to deforming forces, and in elderly patients with pre-existing cervical degenerative changes, such as spondylosis

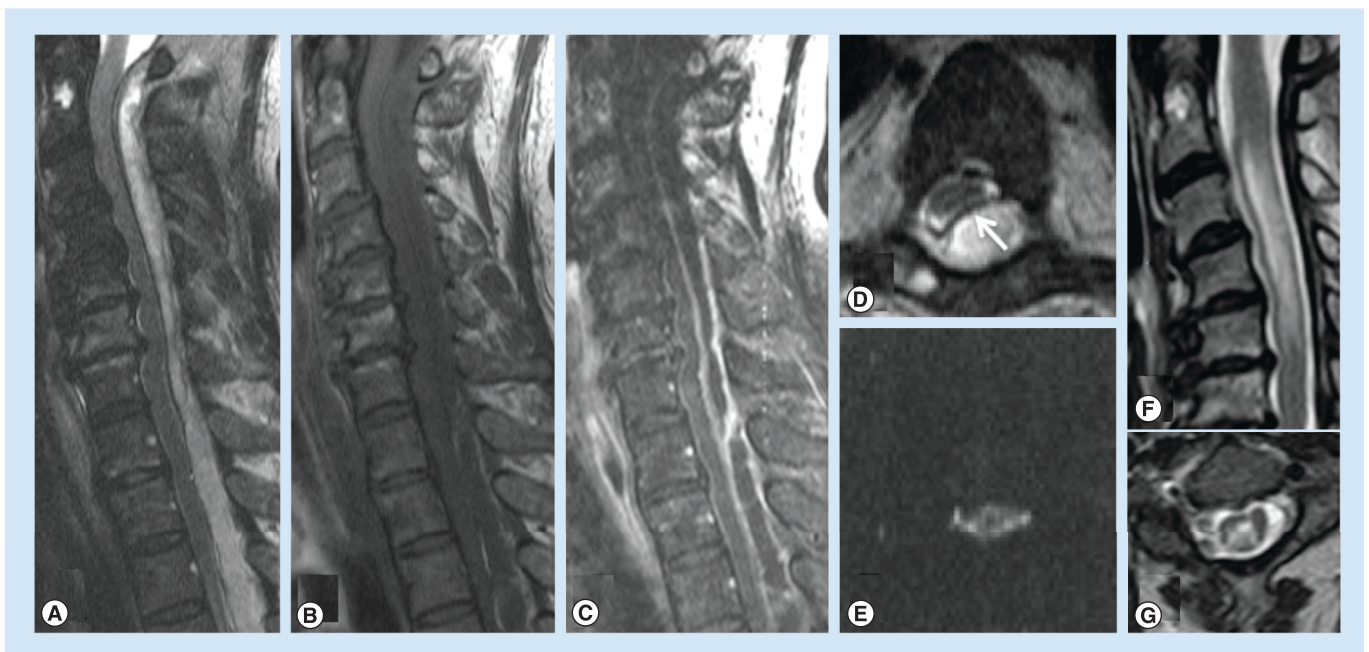


Figure 18. Epidural abscess with spinal cord compression. (A) Sagittal turbo spin echo images show an extensive posterior epidural collection, hyperintense on T₂-weighted image, (B) hypointense on T₁-weighted image with (C) peripheral enhancement on fat-suppressed enhanced T₁-weighted image. (D) Axial turbo spin echo fat-suppressed T₂-weighted image depicts the extradural location of the fluid collection well, with anterior displacement of the dura (arrow on D), and the mass effect on the spinal cord. (E) Axial diffusion-weighted image shows high signal intensity within the extradural abscess. (F & G) display the cord swelling and edema, well visible after surgical decompression of the abscess, despite resolution of the spinal cord compression (also see Figure 4).

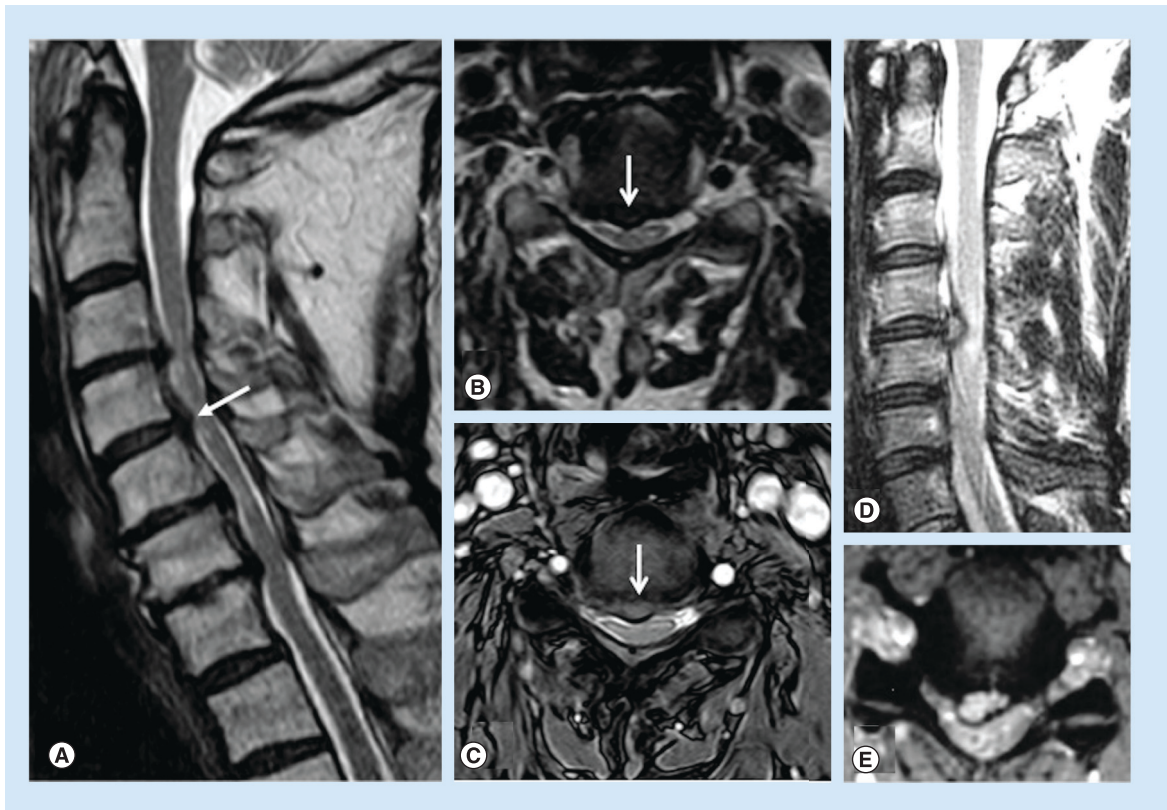


Figure 19. Disc herniations. (A–C) Case 1 with (A) sagittal and (B) axial turbo spin echo T_2 -weighted images showing multilevel cervical spondylotic changes with disc/osteophytes complexes, central canal stenosis, cord compression and apparently chronic myelopathic changes. Note that on turbo spin echo, soft disc herniations and disc–osteophyte complexes are not easily differentiated because both appear T_2 -hypointense (arrows on A & B). In such cases, (C) the corresponding axial gradient-recalled echo T_2 -weighted image depicts the soft disc component as hyperintense (arrow on C), while an osteophyte would have appeared markedly hypointense. (D & E) Case 2 displays a large acute traumatic disc herniation compressing the spinal cord. Note the very high T_2 signal in the disc fragment due to high water content, and the ill-defined high T_2 signal in the cord, meaning cord edema, on the (E) axial gradient-recalled echo T_2 -weighted image.

or disc herniation, resulting in narrowing of the sagittal diameter of the spinal canal. Impingement of the cervical cord by these degenerative changes may explain the mechanism of spinal cord injury in these cases [73–75].

Causes of SCC from the epidural compartment

Epidural hematoma

EDHs are frequently encountered in the setting of spinal trauma or after spinal surgery [76,77]; spontaneous EDHs are rare, generally occurring in older patients (aged 50–80 years) with risk factors such as coagulopathy [78]. Since the dura is not firmly attached to the bones in the spine, EDHs can also derive from low pressure bleeding phenomena, such as venous hemorrhages. The imaging characteristics of EDH vary with the oxidative state of the hemorrhage and the clot retraction. MDCT, providing the first imaging findings in the trauma setting, with the soft tissue window setting, is often helpful in detecting the hyperdense,

frequently crescent-shaped acute hematoma; however, MDCT might suffer from low sensitivity in regions with artifacts or when the EDH is isodense. MRI is regarded as the imaging modality of choice to evaluate EDH; depending on the status of the hemoglobin breakdown products, EDHs have variable signal intensity, from isointense to hyperintense on T_1 -weighted sequences, and from hypointense to hyperintense on T_2 -weighted sequences (Supplementary Figure 7).

For EDHs that appear hyperintense on T_1 - and T_2 -weighted sequences, fat suppression, also applied to the nonenhanced T_1 - and T_2 -weighted images, allows better depiction of the extension of the hematoma against the dark background of the suppressed fat signal, and better appreciation of the relationship with surrounding structures (Figure 16) [79].

Hematomas generally do not show significant enhancement (Supplementary Figure 7), especially in the early stages; this can be an important diagnostic finding in differentiating these lesions from abscess or tumor.

Epidural abscess

Epidural abscess is a dreadful complication of spondylodiscitis. The phlegmon is usually isointense or hypointense on T_1 -weighted images, hyperintense on T_2 -weighted images, with peripheral enhancement after gadolinium injection [80]. Fat-suppressed T_2 -weighted and contrast-enhanced T_1 -weighted sequences are helpful to highlight the infectious site of origin which is often the disc space and subchondral areas along the disc endplates (Figure 17), and to depict the typical peripheral enhancement and central fluid component of the collection (Figure 18) [19]. The contrast-enhancing area often extends in the adjacent soft tissues, beyond the peripheral collection rim, indicating the phlegmonous component, characterized by inflammatory response and edema (Supplementary Figure 8). Recently, DWI has been used to study epidural abscesses; the purulent fluid collection, when the causative agent is a pyogenic germ, appears markedly hyperintense on DWI (Figure 18), and hypointense on the corresponding apparent diffusion coefficient map [81].

CT is performed as a complementary imaging study, generally when MRI is not available or contraindicated. It can render additional information on erosive changes of the bones, especially along the disc endplates in case of spondylodiscitis, and it is also a valuable guide for percutaneous biopsies (Figure 17) [82].

Disc herniations & synovial cysts

Disc herniations are among the most commonly encountered findings in MRI of the cervical and lumbar spine, less commonly found in the thoracic spine. A common

cause of radicular symptoms and signs, due to direct compressive effects and/or local inflammatory response, they are more rarely cause of SCC. Through the rupture or fissuration of the annulus fibrosus and posterior longitudinal ligament, as a result of trauma or much more frequently in relation to degenerative phenomena, extruded disc material may extend into the epidural space causing cord compression. The herniating disc material can be contained by some residual fibers of the stretched and deformed annulus, or be completely extruded in the epidural space. Large disc herniations or a combination of disc herniation on a pre-existing central canal stenosis can cause significant SCC (Figure 19). Sagittal and axial T_2 -weighted images depict the disc herniation, characterize it on the base of the morphology and continuity with the parent disc as contained or extruded, assess the mass effect on the spinal cord, and the presence of cord edema. The signal of the disc fragment can be variable, usually depending on the hydration status of the nuclear material. It is important to note that the herniated disc fragment can display a signal different from the parent disc. The use of gradient echo pulse sequences performed on the axial plane greatly enhances the ability to obtain diagnostic images for the clinical evaluation of cervical disc herniation, offering a sharp delineation of bone/osteophytes, that show low signal, and disc margin, with high signal (Figure 19), an excellent contrast between the spinal cord and surrounding subarachnoid space, and clear visualization of the neural foramina and exiting nerve roots (Figure 19) [83,84]. In case a contrast agent is injected, the disc fragment can have a peripheral rim of enhancement, better visible on fat-suppressed

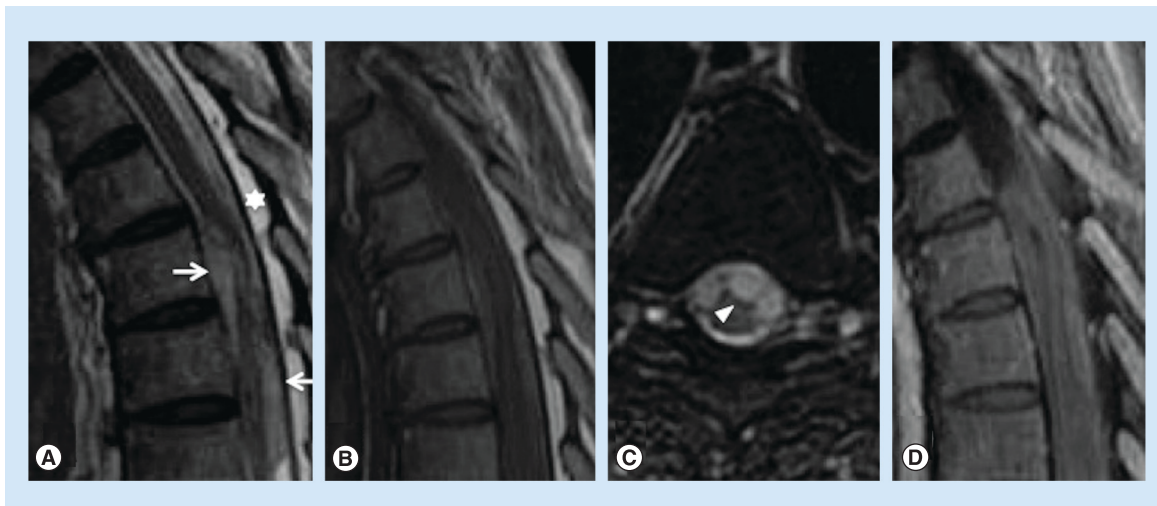


Figure 20. Subdural hematoma. (A) Sagittal turbo spin echo T_2 -weighted image and (B) T_1 -weighted image show a hyperintense collection into the thoracic subdural space (arrows in A). It is located anteriorly to the posterior epidural fat (asterisk) and compresses the spinal cord. (C) Axial turbo spin echo T_2 -weighted image with fat suppression reveals a circumferential disposition of the collection around the thecal sac with a festonated appearance (arrowhead in C); (D) no contrast enhancement is evident on sagittal postcontrast image with fat suppression.

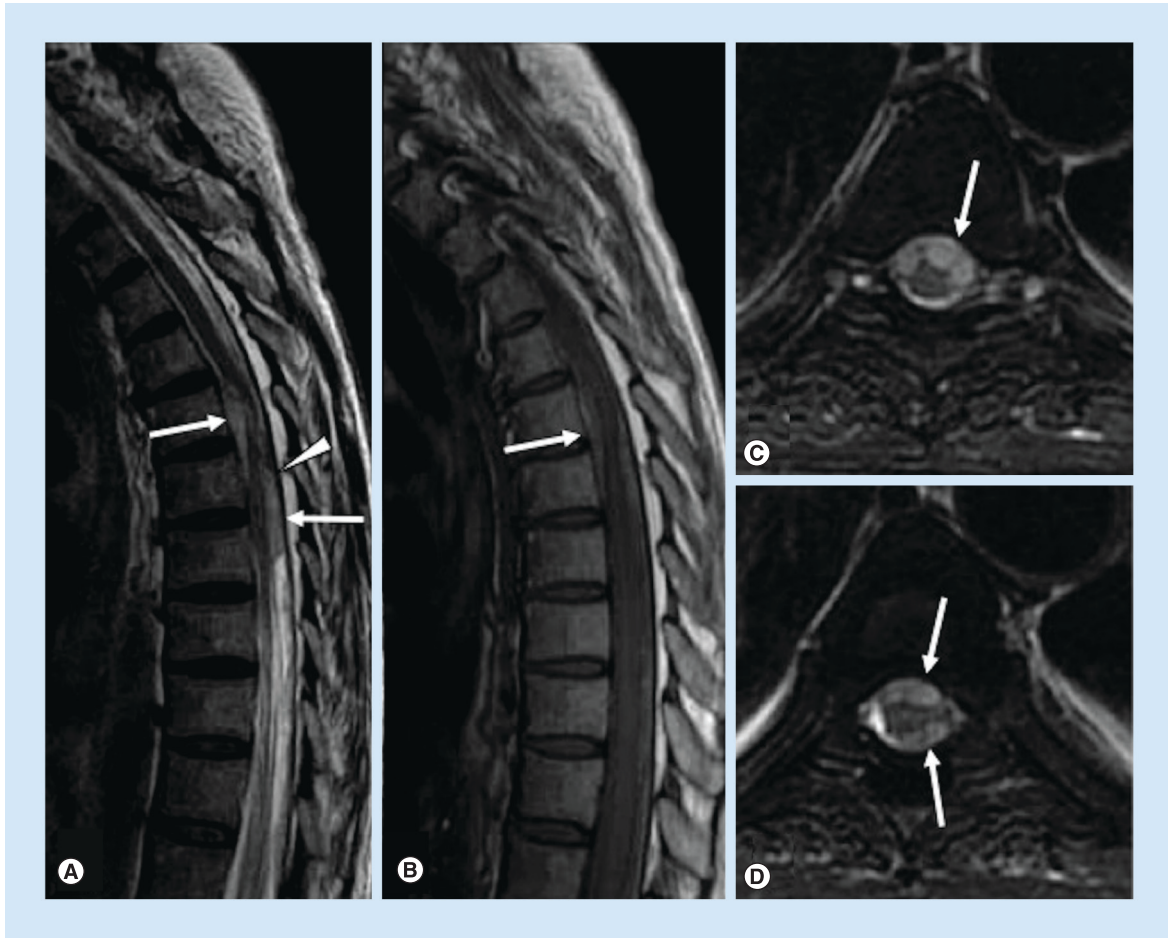


Figure 21. Subdural hematoma. (A) Sagittal turbo spin echo T_2 - and (B) T_1 -weighted images show a hyperintense intradural extramedullary collection anterior and posterior to the spinal cord (arrows in A & B). The thin dark dural line is seen at its place (arrowhead in A), defining the intradural location of the collection. (C & D) Axial turbo spin echo fat-suppressed T_2 -weighted images reveal a circumferential disposition of the collection around the spinal cord with a festonated appearance (arrows in C & D).

enhanced T_1 -weighted images, which might help in the differential diagnosis with a neoplastic mass, such as a meningioma or a schwannoma.

A rarer entity, especially in the cervical and thoracic spine, which can represent a cause of SCC from the epidural space, is the synovial cyst. It most commonly arises in the setting of degenerative changes and originates from the facet joints. If the synovial cyst spurs from the anterior and medial margin of the articular capsule and grows in the central canal, it can compress the spinal cord from the postero-lateral epidural space. The clearest diagnosis of a synovial cyst is provided by MRI, which characteristically shows a well-circumscribed cystic mass, with a fluid-like signal on T_1 - and T_2 -weighted images, typically with a thin capsule and no contrast enhancement [85]. Variations to these typical features are possible, with cysts showing calcific walls, hyperproteinaceous fluid content, with high T_1 - and low T_2 signals. Axial T_2 -weighted images again demonstrate the cyst, its relationship with the facet joint, its epidural loca-

tion, mass effect on the spinal cord, and imaging signs of myelopathy when present. A diagnostic doubt can sometimes be cleared by CT-guided injection of contrast agent in the facet joint space, resulting in contrast opacification of the cyst.

Extramedullary hematopoiesis

Extramedullary hematopoiesis (EMH) is a physiologic response to chronic anemia observed in various hematologic disorders, such as thalassemias, myelofibrosis and polycythemia [86]. EMH is commonly seen in the abdomen or chest, rarely in the epidural space [87]. MRI is obviously the first selected imaging modality for the diagnosis of EMH, clearly showing the site and extent of the lesion in relation to the displaced spinal cord. Active recent hematopoietic extramedullary lesions have rich vasculature, while inactive older lesions have more fatty tissue and iron deposits [88]. If the patient is treated with blood transfusions, the lesion may decrease in size and

appear on MRI with massive iron deposition. Active lesions show intermediate signal intensity in both T_1 - and T_2 -weighted MRI; enhancement is minimal or absent differentiating it from other epidural lesions such as abscesses or metastases. Older inactive lesions show high signal intensity in both T_1 - and T_2 -weighted MRI due to fatty infiltration or low signal intensity in both T_1 - and T_2 -weighted MRI due to iron deposition.

Angiolipoma

Angiolipoma of the spine is a benign neoplasm consisting of both mature fatty tissue and abnormal vascular elements, usually characterized by a slow progressive clinical course [89]. Because angiolipomas are mostly hyperintense on T_1 -weighted images and often nearly isointense with epidural fat, fat-suppression MRI is particularly well suited for the investigation of these tumors. The lesion can also present a variable grade of hypointensity, predictive of its degree of vascularity, likely to be encountered at surgery [90]. On T_2 -weighted images, the tumors have variable signal intensity attributed to the variable vascular and adi-

pose elements of the tumor and most lesions enhance after gadolinium administration.

Causes of SCC from the intradural compartment

Spinal subdural hematoma

Spinal subdural hematoma (SSDH) are contained within the virtual space existing between the apposed dural and arachnoidal meningeal sheets. They can be caused by abnormalities of coagulation, blood dyscrasias, trauma, underlying neoplasm and arteriovenous malformation, and invasive spinal procedures [91]. MRI is the preferred imaging modality to evaluate subdural hematomas. It provides information on their location, extent, morphology and variable T_1 and T_2 signals related to hemoglobin's breakdown products. A SSDH is recognized and distinguished by an EDH by the observation that the thin T_2 -hypointense line of the dura is not displaced and the T_1 -hyperintense epidural fat is regularly seen. SSDH can extend circumferentially inside and along the borders of the thecal sac, by which it possibly causes SCC, and displays a typical appearance on axial images (Figures 20 & 21) [92].

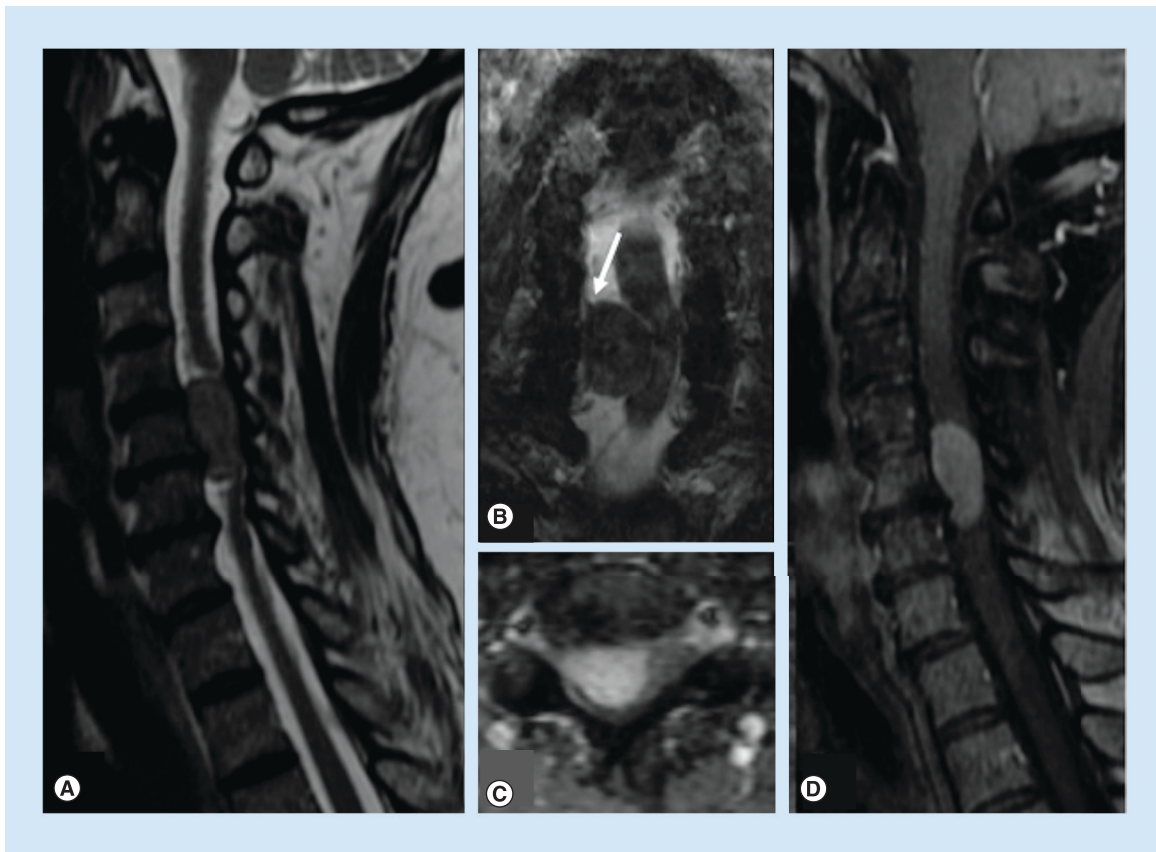


Figure 22. Meningioma. (A) Sagittal turbo spin echo T_2 -weighted, (B) coronal 3D constructive interference in the steady state and (C) axial and (D) sagittal turbo spin echo fat-suppressed enhanced T_1 -weighted images show an expansile intradural-extramedullary mass with homogeneous enhancement laterally displacing the spinal cord. Small dural tail is apparent on high-resolution 3D constructive interference in the steady state image (arrow on B).

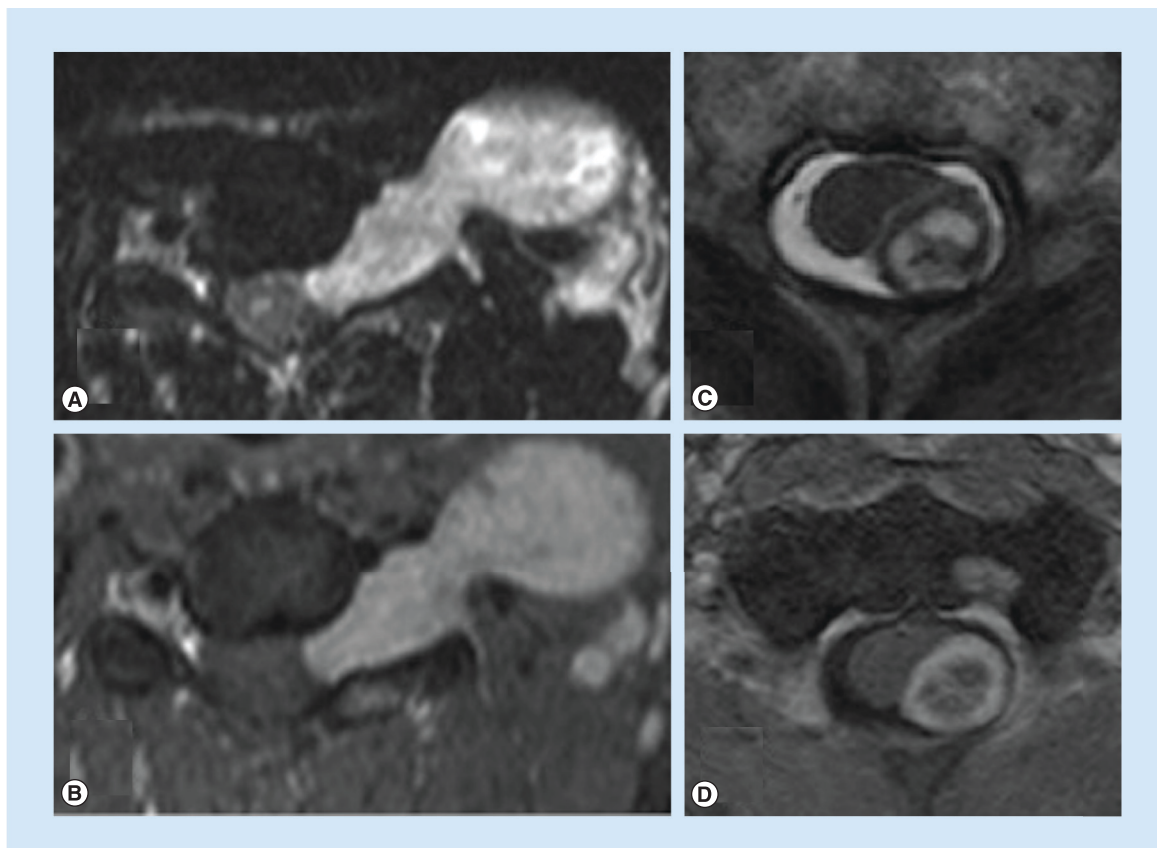


Figure 23. Two different cases of cervical spinal nerve schwannomas. (A) Axial fat-suppressed turbo spin echo T_2 -weighted and (B) enhanced T_1 -weighted images reveal an intensely enhancing, well-margined mass in the central canal and along the course of exiting nerve root in the neural foramen, that is widened. (C) Axial fat-suppressed turbo spin echo T_2 -weighted and (D) enhanced T_1 -weighted images show a rounded, well-defined intradural extramedullary mass with inhomogeneous enhancement compressing the spinal cord.

Primary neoplasms

Intradural–extramedullary tumors lie within the dural borders of the thecal sac, but outside of the spinal cord. Meningioma and schwannoma are the most common primary tumors in this location. These are expansile masses contained by the T_2 -hypointense thin dural line, that determine extrinsic dislocation/compression of the spinal cord, that does not appear enlarged, differently from intramedullary tumors. The epidural fat lining, visible as a T_1 -hyperintense rim around the thecal sac, is preserved. CT can be helpful in defining mineralization or bone remodeling in these tumors, but MRI with multiplanar T_2 -weighted and contrast-enhanced T_1 -weighted sequences, clearly defines tissue characteristics better, the soft tissue planes and neural structures surrounding these lesions. In consideration of the intradural location of these masses, the background to mass contrast is assured by the presence of the CSF, therefore, in theory, use of fat-suppression techniques should not be necessary; although, in practical terms, if a mass is large enough to expand the thecal sac, the borders of the mass may be very close to the adipous epidural compartment,

and still fat suppression applied to the T_2 -weighted and to the contrast-enhanced T_1 -weighted sequences helps to delineate the real borders of the mass. Imaging differentiation of meningioma from schwannoma is not always easy. T_1 and T_2 signal characteristics often overlap, with schwannomas demonstrating slightly more heterogeneously increased T_2 signals. Dural tail and calcifications are predictors of meningioma, whereas an expansile-enhancing mass, extending across the intervertebral foramen, is strongly suggestive of a neural sheet tumor, although meningiomas are also known to display this behavior (Figures 22 & 23) [93,94].

Intradural & leptomeningeal metastasis

The subarachnoid space is a frequent localization for metastatic deposits. MRI is the preferred imaging modality [95] able to demonstrate region of bulky disease, represented by intradural and extramedullary nodules, to visualize clumping of nerve root and spinal cord alterations. In a patient being investigated for suspected SCC, the T_2 -weighted sequence may show a dislocation/compression of the spinal cord and high signal

within it, due to edema adjacent to a pathological extramedullary deposit. The demonstration of intradural metastasis and leptomeningeal lesions is easily obtained on conventional postcontrast T_1 -weighted images, but the use of the postcontrast images with fat suppression increases the evidence of leptomeningeal linear and nodular enhancement areas along the spinal cord surface and nerve roots, resulting in better differentiation from dural thickening/enhancement [19]. In the case of infectious and inflammatory processes, the pattern of enhancement is usually linear and uniform, whereas it tends to be thicker and nodular in cases of tumor spread. The appearance of advanced leptomeningeal carcinomatosis, characterized by thick perimedullary and perineural enhancement, has been described as 'sugar coating' for its appearance on contrast-enhanced T_1 -weighted images (Figure 24) [96].

Arachnoid cyst

Spinal arachnoid cysts are rare lesions most often located in the mid-to-lower thoracic spine. Most spinal arachnoid cysts are asymptomatic and discovered

incidentally by MRI; neuropathic pain, numbness, weakness and myelopathy can be present due to mass effect on the spinal cord [97]. MRI is the imaging modality of choice to assess the size, nature and extent of cystic lesion, as well as the mass effect on the cord (Figure 25) [98,99]. On T_1 - and T_2 -weighted images, the signal within a cyst has the same intensity as CSF. On thin axial T_2 -weighted images, it is possible to assess the mass effect upon the spinal cord, and the possibly associated MRI signs of myelopathy, such as edema and gliosis. High-resolution thin sections (<1 mm) myelographic MRI pulse sequences, heavily fluid sensitive, can precisely depict the cyst walls. The spinal cord can appear flattened. Large cysts can display flow-related artifacts, caused by transmitted pulsations from the circulating CSF. CT can be helpful to assess the remodeling of bone canal determined by the cyst. CT myelography can be used as a complementary and often confirmatory exam, since it may demonstrate or exclude a communication between the subarachnoid space and the cyst, which is important for surgical planning [100].



Figure 24. Two cases of meningeal metastasis. (A) A turbo spin echo fat-suppressed enhanced T_1 -weighted image shows dural nodular-enhancing deposits compressing the spinal cord, in this patient with primary lung cancer. (B & C) Sagittal turbo spin echo T_2 -weighted and fat-suppressed enhanced T_1 -weighted images show extensive bulky subarachnoid leptomeningeal carcinomatosis, compressing the spinal cord, from a myxopapillary ependymoma.

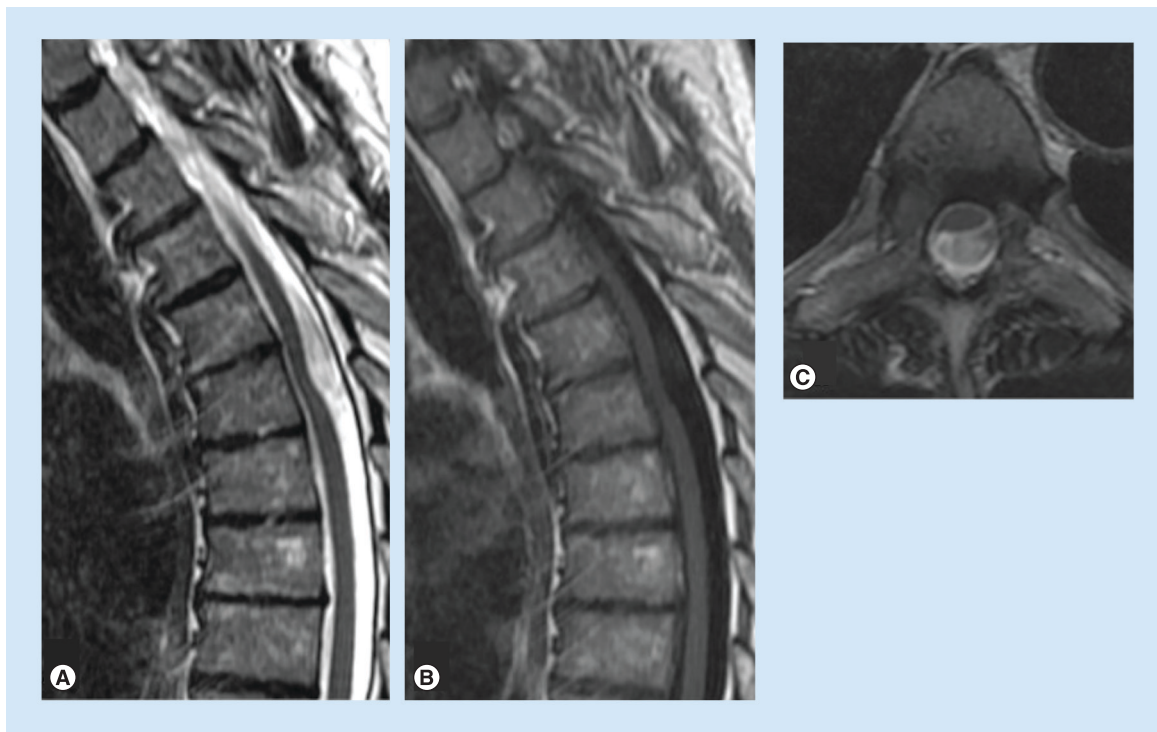


Figure 25. Arachnoid cyst. (A) Sagittal turbo spin echo T_2 - and (B) T_1 -weighted images demonstrate a posterior mid thoracic cyst with the same signal as cerebrospinal fluid compressing the spinal cord anteriorly. (C) The axial turbo spin echo T_2 -weighted image shows the flattening of the posterior aspect of the cord.

Neuroenteric cyst

Neuroenteric cysts are rare congenital epithelium-lined cysts of the CNS [101]; they are usually located anteriorly to the spinal cord. The most common myelographic and CT myelographic appearance is that of a lobulated intradural–extramedullary mass. Neuroenteric cysts are usually isointense to hyperintense relative to CSF on long repetition time sequences and isointense or slightly hyperintense to CSF on T_1 -weighted images. These signal characteristics correlate with the high-protein-content fluid within the cysts, described at surgery as milky or mucinous [102].

Intramedullary lesion

An enlargement of the spinal cord, due to vascular, neoplastic or inflammatory processes, may determine an obliteration of CSF surrounding the spinal cord, causing a SCC through a vicious circle of congestive myelopathy.

Conclusion

Imaging is essential to confirm and characterize a clinical suspect of SCC. CT is the preferred imaging modality to assess bone structures, especially in the trauma setting, whereas MRI is advantageous in the evaluation of soft tissues and is unique in the visualization of spinal cord, both in acute, sub-

acute and chronic settings. For a schematic approach to the imaging differential diagnosis of the various causes of SCC, it is important to determine the site of origin of the lesion, whether from the osseous, epidural, or intradural compartment in the spine. Further research will likely bring to the clinical arena advanced microstructural imaging techniques able to provide diagnostic and prognostic information in various SCC conditions.

Future perspective

Recent technological advances (e.g., DWI, DTI and tractography) will likely be able to further characterize neural tissue at a microstructural level, predicting tissue viability, functional prognosis and patient recovery.

Financial & competing interests disclosure

The authors have no relevant affiliations or financial involvement with any organization or entity with a financial interest in or financial conflict with the subject matter or materials discussed in the manuscript. This includes employment, consultancies, honoraria, stock ownership or options, expert testimony, grants or patents received or pending, or royalties.

No writing assistance was utilized in the production of this manuscript.

Executive summary

Imaging in spinal cord compression

- Multidetector CT (MDCT) is the preferred imaging modality to assess bone structures especially in acute trauma patients and absolutely needs diagnostic complement by MRI when spinal cord compression (SCC) is suspected. MRI can be considered as the first-line imaging method in all other nontraumatic spinal cord syndromes in which SCC needs to be ruled out.

Strategies to approach SCC

- SCC may be caused by different pathologies arising from or involving different anatomical compartments. The recognition of the lesions' compartment of origin narrows the broad spectrum of differential diagnosis.

Anatomically based causes of SCC

- From the osseous compartment: traumatic fractures and dislocations, osteoporotic and pathologic fractures, vertebral neoplasms, aggressive hemangioma and degenerative changes such as vertebral posterior osteophytes, disc-osteophyte complexes, ligamentous calcification and ossification, articular masses hypertrophy, and antero/retrolisthesis.
- From the epidural compartment: hematoma, abscess, disc herniations and synovial cyst.
- From intradural compartment: subdural hematoma, primary neoplasms, intradural and leptomeningeal metastasis.

References

Papers of special note have been highlighted as:

- of considerable interest
- 1 Kirshblum SC, Waring W, Blering-Sorensen F *et al.* Reference for the 2011 revision of the international standards for neurological classification of spinal cord injury. *J. Spinal Cord Med.* 34(6), 547–554 (2011).
- 2 O'Phelan KH, Bunney EB, Weingart SD, Smith WS. Emergency neurological life support: spinal cord compression (SCC). *Neurocrit. Care* 17(Suppl. 1), S96–S101 (2012).
- 3 Shelerud RA, Paynter KS. Rarer causes of radiculopathy: spinal tumors, infections, and other unusual causes. *Phys. Med. Rehabil. Clin. N. Am.* 13(3), 645–696 (2002).
- 4 Seidenwurm DJ, Wippold FJ 2nd, Cornelius RS *et al.* ACR appropriateness criteria myelopathy. *J. Am. Coll. Radiol.* 9(5), 315–324 (2012).
- Discusses various imaging modalities used in different clinical contexts of myelopathy.
- 5 Geijer M, El-Khoury GY. MDCT in the evaluation of skeletal trauma: principles, protocols, and clinical applications. *Emerg. Radiol.* 13(1), 7–18 (2006).
- 6 Li AE, Fishman E. Cervical spine trauma: evaluation by multidetector CT and three dimensional volume rendering. *Emerg. Radiol.* 10(1), 34–39 (2003).
- 7 Post MJ, Becerra JL, Madsen PW *et al.* Acute spinal subdural hematoma: MR and CT findings with pathologic correlates. *Am. J. Neuroradiol.* 15(10), 1895–905 (1994).
- 8 MacVicar D. Imaging of the spine in patients with malignancy. *Cancer Imaging.* 31(6), S22–S26 (2006).
- 9 Kalichman L, Kim DH, Li L *et al.* Computed tomography-evaluated features of spinal degeneration: prevalence, intercorrelation, and association with self-reported low back pain. *Spine* 10(3), 200–208 (2010).
- 10 Thornbury JR, Fryback DG, Turski PA *et al.* Disk-caused nerve compression in patients with acute low-back pain: diagnosis with MR, CT myelography and plain CT. *Radiology* 186, 731–738 (1993).
- 11 Keith J, Kaste SC. The ALARA (as low as reasonably achievable) concept in pediatric interventional and fluoroscopic imaging: striving to keep radiation doses as low as possible during fluoroscopy of pediatric patients – a white paper executive summary. *Radiology* 240, 621–622 (2006).
- 12 Geijer M, El-Khoury GY. MDCT in the evaluation of skeletal trauma: principles, protocols, and clinical applications. *Emerg. Radiol.* 13, 7–18 (2006).
- 13 Martin E, Prasarn N, Coyne E *et al.* Inpatient radiation exposure in patients with spinal trauma. *J. Spinal Cord Med.* 36, 112–117 (2013).
- 14 Goldberg AL, Kershaw SM. Advances in imaging of vertebral and spinal cord injury. *J. Spinal Cord Med.* 33(2), 105–116 (2010).
- 15 Kremer S, Holl N, Schmitt E *et al.* Imaging of non-traumatic and non tumoral cord lesions. *J. Radiol.* 91, 969–987 (2010).
- 16 Green C, Butler J, Eustace S *et al.* Imaging modalities for cervical spondylotic stenosis and myelopathy. *Adv. Orthop.* 2012, 908324 (2012).
- 17 Neuhold A, Stiskal M, Platzer CH *et al.* Combined use of spin-echo and gradient-echo MR-imaging in cervical disk disease. *Neuroradiology* 33(5), 422–426 (1991).
- 18 Kasdan RB, Howard JL. Neuroimaging of spinal diseases: a pictorial review. *Semin. Neurol.* 28, 570–589 (2008).
- 19 Colosimo C, Cianfoni A, Di Lella GM, Gaudino S. Contrast-enhanced MR imaging of the spine: when, why and how? *Neuroradiology* 1, 18–33 (2006).
- 20 Kato A, Ushio Y, Hayakawa T. Circulatory disturbance of the spinal cord with epidural neoplasm in rats. *J. Neurosurg.* 63, 260–265 (1985).
- 21 Holtz A, Nyström B, Gerdin B *et al.* Neuropathological changes and neurological function after spinal cord compression in the rat. *J. Neurotrauma* 7(3), 155–167 (1990).
- 22 Chen CJ, Hsu HL, Niu CC *et al.* Cervical degenerative disease at flexion-extension MR imaging: prediction criteria. *Radiology* 227(1), 136–142 (2003).
- 23 Vargas MC, Castillo M. Magnetic resonance imaging in Hirayama disease. *J. Radiol. Case Rep.* 5(3), 17–23 (2011).
- 24 Stroman PW, Bosma RL, Kornelsen J *et al.* Advanced MR imaging techniques and characterization of residual anatomy. *Clin. Neurol. Neurosurg.* 114(5), 460–470 (2012).

- 25 Demir A, Ries M, Moonen CT *et al.* Diffusion-weighted MR imaging with apparent diffusion coefficient and apparent diffusion tensor maps in cervical spondylotic myelopathy. *Radiology* 229(1), 37–43 (2003).
- 26 Thurnher MM, Law M. Diffusion-weighted imaging, diffusion-tensor imaging, and fiber tractography of the spinal cord. *Magn. Reson. Imaging Clin. N. Am.* 17(2), 225–244 (2009).
- Describes some applications of diffusion-weighted imaging and diffusion-tensor imaging in the evaluation of spinal cord diseases.
- 27 Lee JW, Kim JH, Park JB *et al.* Diffusion tensor imaging and fiber tractography in cervical compressive myelopathy: preliminary results. *Skeletal Radiol.* 40(12), 1543–1551 (2011).
- 28 Jones JG, Cen SY, Lebel RM *et al.* Diffusion tensor imaging correlates with the clinical assessment of disease severity in cervical spondylotic myelopathy and predicts outcome following surgery. *Am. J. Neuroradiol.* 34(2), 471–478 (2013).
- Investigates the potential use of diffusion-tensor imaging to assess disease severity and to predict outcome in cervical spondylotic myelopathy.
- 29 Song KJ, Choi BW, Kim GH, Kim JR. Clinical usefulness of CT-myelogram comparing with the MRI in degenerative cervical spinal disorders is CTM still useful for primary diagnostic tool? *J. Spinal Disord. Tech.* 22(5), 353–357 (2009).
- 30 Antevil JL, Sise MJ, Sack DI *et al.* Spiral computed tomography for the initial evaluation of spine trauma: a new standard of care? *J. Trauma* 61(2), 382–387 (2006).
- 31 Geijer M, El-Khoury GY. MDCT in the evaluation of skeletal trauma: principles, protocols and clinical applications. *Emerg. Radiol.* 13(1), 7–18 (2006).
- 32 Panczykowski DM, Tomycz ND, Okonkwo DO. Comparative effectiveness of using computed tomography alone to exclude cervical spinal injuries in obtunded or intubated patients: meta-analysis of 14,327 patients with blunt trauma. *J. Neurosurg.* 115(3), 541–549 (2011).
- 33 Plumb JO, Morris CG. Clinical review: spinal imaging for the adult obtunded blunt trauma patient: update from 2004. *Intensive Care Med.* 38(5), 752–771 (2012).
- 34 Lammertse D, Dungan D, Dreisbach J *et al.* Neuroimaging in traumatic spinal cord injury: an evidence-based review for clinical practice and research. *J. Spinal Cord Med.* 30, 205–214 (2007).
- 35 Quint DJ. Indications for emergent MRI of the central nervous system. *JAMA* 283, 853–855 (2000).
- 36 Forster BB, Koopmans RA. Magnetic resonance imaging of acute trauma of the cervical spine: spectrum of findings. *Can. Assoc. Radiol. J.* 46(3), 168–173 (1995).
- 37 Looby S, Flanders A. Spine trauma. *Radiol. Clin. North Am.* 49(1), 129–163 (2011).
- 38 Saifuddin A. MRI of acute spinal trauma. *Skeletal Radiol.* 30(5), 237–246 (2001).
- 39 Saifuddin A, Noordeen H, Taylor BA, Bayley I. The role of imaging in the diagnosis and management of thoracolumbar burst fractures: current concepts and a review of the literature. *Skeletal Radiol.* 25(7), 603–613 (1996).
- 40 Dai LY, Ding WG, Wang XY *et al.* Assessment of ligamentous injury in patients with thoracolumbar burst fractures using MRI. *J. Trauma* 66(6), 1610–1615 (2009).
- 41 Lemons VR, Wagner FC Jr, Montesano PX. Management of thoracolumbar fractures with accompanying neurologic injury. *Neurosurgery* 30(5), 667–671 (1992).
- 42 Chandra J, Sheerin F, Lopez de Heredia L *et al.* MRI in acute and subacute post-traumatic spinal cord injury: pictorial review. *Spinal Cord* 50(1), 2–7 (2012).
- 43 Leypold BG, Flanders AE, Burns AS. The early evolution of spinal cord lesions on MR imaging following traumatic spinal cord injury. *Am. J. Neuroradiol.* 29(5), 1012–1016 (2008).
- 44 Cianfoni A, Colosimo C. Imaging of spine trauma. In: *Problem Solving in Neuroradiology*. Elsevier, Amsterdam, The Netherlands, 13, 487–488 (2011).
- 45 Silberstein M, Tress BM, Hennessy O. Prediction of neurologic outcome in acute spinal cord injury: the role of CT and MR. *Am. J. Neuroradiol.* 13(6), 1597–608 (1992).
- 46 Heggness MH. Osteoporotic fractures rarely cause spinal cord compression. *Osteoporosis Int.* 3(4), 215–221 (1993).
- 47 Uetani M, Hashmi R, Hayshi K. Malignant and benign compression fractures: differentiation and diagnostic pitfalls on MRI. *Clin. Radiol.* 59(2), 124–131 (2004).
- 48 Schiff D. Spinal cord compression. *Neurol. Clin. N. Am.* 21, 67–86 (2003).
- 49 MacVicar D. Imaging of the spine in patients with malignancy. *Cancer Imaging* 6, S22–S26 (2006).
- 50 Kim DH, Rosenblum JK, Panghaal VS *et al.* Differentiating neoplastic from non neoplastic processes in the anterior extradural space. *Radiology* 260(3), 825–830 (2011).
- 51 Cianfoni A, Massari F, Dani G *et al.* Percutaneous ethanol embolization and cement augmentation of aggressive vertebral hemangiomas of two adjacent vertebral levels. *J. Neuroradiol.* doi:10.1016/j.neurad.2012.10.003 (2013) (Epub ahead of print).
- 52 Cross JJ, Antoun NM, Laing RJ, Xuereb J. Imaging of compressive vertebral haemangiomas. *Eur. Radiol.* 10(6), 997–1002 (2000).
- 53 Yukawa Y, Kato F, Yoshihara H *et al.* MR T₂ image classification in cervical compression myelopathy: predictor of surgical outcomes. *Spine* 32(15), 1675–1678 (2007).
- 54 Matsumoto M, Toyama Y, Ishikawa M *et al.* Increased signal intensity of the spinal cord on magnetic resonance images in cervical compressive myelopathy: does it predict the outcome of conservative treatment? *Spine* 25(6), 677–682 (2000).
- 55 Hackney DB, Asato R, Joseph PM *et al.* Hemorrhage and edema in acute spinal cord compression: demonstration by MRI. *Radiology* 161(2), 387–390 (1986).
- 56 Matsuda Y, Miyazaki K, Tada K *et al.* Increased MR signal intensity due to cervical myelopathy. Analysis of 29 surgical cases. *J. Neurosurg.* 74(6), 887–892 (1991).
- 57 Mehalic TF, Pezzuti RT, Applebaum BI. Magnetic resonance imaging and cervical spondylotic myelopathy. *Neurosurgery* 26(2), 217–226 (1990).

- 58 Okada Y, Ikata T, Yamada H, Sakamoto R, Katoh S. Magnetic resonance imaging study on the results of surgery for cervical myelopathy. *Spine* 18(14), 2024–2029 (1993).
- 59 Ohshio I, Hatayama A, Kaneda K *et al.* Correlation between histopathologic features and magnetic resonance images of spinal cord lesions. *Spine* 18, 1140–1149 (1993).
- 60 Chen CJ, Lyu RK, Lee ST *et al.* Intramedullary high signal intensity on T₂ weighted MR images in cervical spondylotic myelopathy: predictors of prognosis with type of intensity. *Radiology* 221(3), 789–794 (2001).
- 61 Wada E, Yonenobu K, Suzuki S *et al.* Can intramedullary signal change on magnetic resonance imaging predict surgical outcome in cervical spondylotic myelopathy. *Spine* 24, 455–461 (1999).
- 62 Mastronardi L, Elsawaf A, Roperto R *et al.* Prognostic relevance of the postoperative evolution of intramedullary spinal cord changes in signal intensity on magnetic resonance imaging after anterior decompression for cervical spondylotic myelopathy. *J. Neurosurg. Spine*. 7(6), 615–622 (2007).
- 63 Shen HX, Li L, Yang ZG *et al.* Position of increased signal intensity in the spinal cord on MR images: does it predict the outcome of cervical spondylotic myelopathy? *Chin. Med. J.* 122912, 1418–1422 (2009).
- 64 Ozawa H, Sato T, Hyodo H *et al.* Clinical significance of intramedullary Gd-DTPA enhancement in cervical myelopathy. *Spinal Cord* 48(5), 415–422 (2009).
- 65 Boet R, Chan YL, King A *et al.* Contrast enhancement of the spinal cord in a patient with cervical spondylotic myelopathy. *J. Clin. Neurosci.* 11(5), 512–514 (2004).
- 66 Cho YE, Shin JJ, Kim KS *et al.* The relevance of intramedullary high signal intensity and gadolinium (Gd-DTPA) enhancement to the clinical outcome in cervical compressive myelopathy. *Eur. Spine J.* 2267–2274 (2011).
- 67 Ducreux D, Fillard P, Facon D *et al.* Diffusion tensor magnetic resonance imaging and fiber tracking in spinal cord lesions: current and future indications. *Neuroimaging Clin. N. Am.* 17(1), 137–147 (2007).
- 68 Lee JW, Park KS, Kim JH *et al.* Diffusion tensor imaging in idiopathic acute transverse myelitis. *Am. J. Roentgenol.* 191(2), W52–W57 (2008).
- 69 Ohgiya Y, Oka M, Hiwatashi A *et al.* Diffusion tensor MR imaging of the cervical spinal cord in patients with multiple sclerosis. *Eur. Radiol.* 7(10), 2499–2504 (2007).
- 70 Demir A, Ries M, Moonen CT *et al.* Diffusion-weighted MR imaging with apparent diffusion coefficient and apparent diffusion tensor maps in cervical spondylotic myelopathy. *Radiology* 229(1), 37–43 (2003).
- 71 Facon D, Ozanne A, Fillard P *et al.* MR diffusion tensor imaging and fiber tracking in spinal cord compression. *Am. J. Neuroradiol.* 26(6), 1587–1594 (2005).
- 72 Tsuchiya K, Katasa S, Fujikawa A *et al.* Diffusion-weighted MRI of the cervical spinal cord using a single-shot fast spin-echo technique: findings in normal subjects and in myelomalacia. *Neuroradiology* 45(2), 90–94 (2003).
- 73 Kothari P, Freeman B, Greivitt M, Kerslake R. Injury to the spinal cord without radiological abnormality (SCIWORA) in adults. *J. Bone Joint Surg. Br.* 82(7), 1034–1037 (2000).
- 74 Gupta S, Rajeev K, Khosla VK *et al.* Spinal cord injury without radiographic abnormality in adults. *Spinal Cord* 37(10), 726–729 (1999).
- 75 Kato H, Kimura A, Sasaki R *et al.* Cervical spinal cord injury without bony injury: a multicenter retrospective study of emergency and critical care centers in Japan. *J. Trauma* 65(2), 373–379 (2008).
- 76 Foo D, Rossier AB. Post-traumatic spinal epidural hematoma. *Neurosurgery* 11(1), 25–32 (1982).
- 77 Sokolowski MJ, Garvey TA, Perl J 2nd *et al.* Prospective study of postoperative lumbar epidural hematoma: incidence and risk factors. *Spine* 33(1), 108–113 (1976).
- 78 Wang VY, Chou D, Chin C. Spine and spinal cord emergencies: vascular and infectious. *Neuroimaging Clin. N. Am.* 20(4), 639–650 (2010).
- 79 Adamson DC, Bulsara K, Bronc PR. Spontaneous cervical epidural hematoma: case report and literature review. *Surg. Neurol.* 62(2), 156–159 (2004).
- 80 Torgovnick J, Sethi N, Wyss J. Spinal epidural abscess: clinical presentation, management, and outcome. *Surg. Neurol.* 64(3), 279 (2005).
- 81 Eastwood JD, Vollmer RT, Provenzale JM. DWI in a patient with vertebral and epidural abscess. *Am. J. Neuroradiol.* 23(3), 496–498 (2002).
- 82 Enoch DA, Cargill JS, Laing R *et al.* Value of CT-guided biopsy in the diagnosis of septic discitis. *J. Clin. Pathol.* 61(6), 750–753 (2008).
- 83 Hedberg MC, Drayer BP, Flom RA *et al.* Gradient echo (GRASS) MR imaging in cervical radiculopathy. *Am. J. Roentgenol.* 150(3), 683–689 (1988).
- 84 Enzmann DR, Rubin JB. Cervical spine: MR imaging with a partial flip angle, gradient-refocused pulse sequence. Part I. General considerations and disk disease. *Radiology* 166(2), 467–472 (1988).
- 85 Jackson DE, Atlas SW Jr, Mani JR, Norman D. Intraspinal synovial cysts: MR imaging. *Radiology* 170(2), 527–530 (1989).
- 86 Cappellini MD, Musallam KM, Taher AT. Insight onto the pathophysiology and clinical complications of thalassemia intermedia. *Hemoglobin* 1, S145–S159 (2009).
- 87 Ghieda U, Elshimy M, El Beltagi AH. Progressive spinal cord compression due to epidural extramedullary hematopoiesis in thalassemia intermedia. A case report and literature review. *Neuroradiol. J.* 26, 111–117 (2013).
- 88 Tsitouridis J, Stamos S, Hassapopoulou E *et al.* Extramedullary paraspinal hematopoiesis in thalassemia: CT and MRI evaluation. *Eur. J. Radiol.* 30, 33–38 (1999).
- 89 Meng J, Du Y, Yang HF *et al.* Thoracic epidural angiolipoma: a case report and review of the literature. *World J. Radiol.* 5, 187–192 (2013).
- 90 Provenzale JM, McLendon RE. Spinal angiolipomas: MR features. *Am. J. Neuroradiol.* 17, 713–719 (1996).
- 91 Dampeer RA. Spontaneous spinal subdural hematoma: case study. *Am. J. Crit. Care* 19(2), 191–193 (2010).
- 92 Montano N, Nucci CG, Doglietto F *et al.* Spontaneous idiopathic spinal subdural hematoma. *Neurology* 71(10), e27 (2008).

- 93 Sevick RJ, Wallace CJ. MR imaging of neoplasms of the lumbar spine. *Magn. Reson. Imaging Clin. N. Am.* 7(3), 539–553 (1990).
- 94 Liu WC, Choi G, Lee SH *et al.* Radiological findings of spinal schwannomas and meningiomas: focus on discrimination of two disease entities. *Eur. Radiol.* 19(11), 2707–2715 (2009).
- 95 Collie DA, Brush JP, Lammie GA *et al.* Imaging features of leptomeningeal metastases. *Clin. Radiol.* 54(11), 765–771 (1999).
- 96 Chamberlain MC. Comparative spine imaging in leptomeningeal metastases. *J. Neurooncol.* 23, 233–238 (1995).
- 97 Dick P. Myelopathy due to spinal arachnoid cyst. *Spine* 11(1), 80–82 (1986).
- 98 Hughes G, Ugokwe K, Benzel EC. A review of spinal arachnoid cysts. *Cleve. Clin. J. Med.* 75(4), 311–315 (2008).
- 99 Liu JK, Cole CD, Kan P *et al.* Spinal extradural arachnoid cysts: clinical, radiological and surgical features. *Neurosurg. Focus* 22(2), E6 (2007).
- 100 Krings T, Lukas R, Reul J. Diagnostic and therapeutic management of spinal arachnoid cysts. *Acta Neurochirurgica* 143(3), 227–234 (2001).
- 101 Cai C, Shen C, Yang W *et al.* Intraspinal neurenteric cysts in children. *Can. J. Neurol. Sci.* 35, 609–615 (2008).
- 102 Brooks BS, Duvall ER, el Gammal T *et al.* Neuroimaging features of neurenteric cysts: analysis of nine cases and review of the literature. *Am. J. Neuroradiol.* 14, 735–746 (1993).